

OPTIMIZING RAMAN SPECTRAL COLLECTION FOR QUARTZ AND ZIRCON
CRYSTALS FOR ELASTIC GEOTHERMOBAROMETRY

by

Mayara F. Cizina



A thesis

submitted in partial fulfillment

of the requirements for the degree of

Master of Science in Geoscience

Boise State University

December 2020

© 2020

Mayara F. Cizina

ALL RIGHTS RESERVED

BOISE STATE UNIVERSITY GRADUATE COLLEGE

DEFENSE COMMITTEE AND FINAL READING APPROVALS

of the thesis submitted by

Mayara F. Cizina

Thesis Title: Optimizing Raman Spectral Collection for Quartz and Zircon Crystals for Elastic Geothermobarometry

Date of Final Oral Examination: 02 October 2020

The following individuals read and discussed the thesis submitted by student Mayara F. Cizina, and they evaluated their presentation and response to questions during the final oral examination. They found that the student passed the final oral examination.

Matthew J. Kohn, Ph.D.	Chair, Supervisory Committee
Karen Viskupic, Ph.D.	Member, Supervisory Committee
T. Dylan Mikesell, Ph.D.	Member, Supervisory Committee
C.J. Northrup, Ph.D.	Member, Supervisory Committee

The final reading approval of the thesis was approved by Matthew J. Kohn, Ph.D., Chair of the Supervisory Committee. The thesis was approved by the Graduate College.

ACKNOWLEDGMENTS

I would like to thank everyone in the Geosciences department that helped grow and achieve my goals in graduate school, specially my advisor, Dr. Matthew Kohn, who was always so kind and patient with all my questions, and helped me improve my writing and communication skills and become a better scientist. To my committee members, Dr. Karen Viskupic, Dr. Dylan Mikesell, and Dr. C.J. Northrup, I appreciate having you in my committee, each of you put valuable input to my research and helped me grow more as a scientist. My gratitude also goes to Pam Cedillo, who helped me with temperature measurements and taught me to appreciate how to build and maintain equipment. I would also like to thank my Geosciences graduate peers that were always there to help me with my research and calm me down when I could not see things clearly. Lastly, I would love to thank Paul Davis, who was extremely important in my research; Paul helped me understand in more details how the Raman microscope worked, and he was always very patient and kind when my experiments went wrong.

ABSTRACT

Raman microspectroscopy is widely used to identify and characterize organic and inorganic compounds. In the geosciences, Raman microspectroscopy has been used to identify mineral and fluid inclusions in host crystals, as well as to calculate pressure-temperature (P-T) conditions using mineral inclusions in host crystals, such as quartz-in-garnet barometry (QuiG). For thermobarometric applications, the reproducibility of Raman peak position measurements is crucial to obtain accurate P-T estimates. In this study, we explored how to optimize Raman spectral collection of quartz and zircon inclusions and reference crystals by monitoring machine stability and by varying spectral parameters. We also monitored a reference Hg atomic-emission line derived from fluorescent lights. Factors that we varied independently included laser source [442 nm (blue), 532 nm (green), 633 nm (red)], power density (1 to 100%) and acquisition time (3 to 270s). Drifting up to 1 cm^{-1} occurred within the first hour of powering the laser source, after which spectra were usually stable for several hours. However, abrupt shifts in peak positions can occur subsequently that can be either positively or negatively correlated to changes in room temperature greater than $0.1 \text{ }^\circ\text{C}$. The Hg-line showed highly correlated but attenuated directional shifts compared to quartz and zircon peaks. Varying spectral parameters did not shift Raman peaks of either quartz or zircon grains. However, some zircon inclusions were damaged at higher power levels of the blue laser source, likely because of laser-induced heating. We also used Raman spectra of a quartz inclusion in garnet collected with blue, green, and red lasers to calculate inclusion pressures (“ P_{inc} ”),

which were then used to calculate inclusion entrapment pressures (“ P_{trap} ”). The published maximum pressure for this rock is c. 0.7 GPa based on thermodynamic calculations. Using a combination of 1, 2, or 3 peaks to calculate P_{inc} and consequently P_{trap} , showed that use of the blue laser source resulted in the most reproducible P_{trap} values for all methods (0.59 to 0.68 GPa), with precisions for a single method as small as ± 0.03 GPa, 2σ). Using the green and red lasers, some methods of calculating P_{trap} gave nearly identical estimates as the blue laser with similarly good precision (± 0.02 GPa for green laser, ± 0.03 GPa for red laser). However, using 1- and 2-peak methods to calculate P_{trap} can yield values that range from 0.52 GPa and 0.53 GPa up to 0.93 GPa and 1.00 GPa for green and red lasers, respectively. For optimal measurements, we recommend: 1) delaying data collection approximately one hour after laser startup, or leave the laser on; 2) collecting the Hg-line simultaneously with Raman spectra of mineral inclusions to correct partially for externally-induced shifts in peak positions, and either 3a) using the blue laser for either quartz or zircon crystals for P-T calculations, but for zircon, using very low laser power (<12 mW) to avoid overheating and damaging of zircon inclusions or 3b) using either the green or red laser for P-T calculations, but to restrict calculations to specific methods. Implementation of our recommendations should contribute to better precision in elastic geothermobarometry, especially QuiG barometry.

TABLE OF CONTENTS

ACKNOWLEDGMENTS	iv
ABSTRACT	v
LIST OF TABLES	ix
LIST OF FIGURES	x
LIST OF ABBREVIATIONS	xiv
INTRODUCTION.....	1
BACKGROUND.....	4
Mineral Inclusion Elastic Barometry	4
Reports on Measurement Protocols	6
METHODS	7
Samples	7
Naming Convention for Peak Positions	7
Raman Measurements	10
Peak Fitting.....	12
Peak to Background Ratio Calculations.....	15
Temperature Measurements	15
Laser Source Comparisons on Quartz and Zircon	16
Entrapment Pressure (P_{trap}) Calculations.....	16
RESULTS	18

Peak Drift	18
1. Initial Drift.....	18
2. Stabilization.....	18
3. Other Slow Drift Periods.....	18
4. Abrupt Changes.	18
5. Shifts to Peak Offsets Relative to External 484 cm ⁻¹ Reference.	19
6. Temperature Correlations.....	19
Effects of Power Density and Total Acquisition Time	21
Zircon Damage Using Blue Excitation Wavelength.....	28
Peak to Background Ratios Using Blue Laser.....	29
Laser Source Comparisons	30
Reproducibilities	30
Differences in Peak Positions Using Different Lasers	32
Quartz Entrapment Pressure Using Different Lasers.....	35
Summary of Reproducibilities	37
DISCUSSION	39
Temporal Drift of Raman Spectra	39
Effects of Power Density and Acquisition Time on Quartz and Zircon	46
Zircon Damage Using Blue Laser Source.....	48
Effect of Laser Frequency on Raman Spectrum Quality	49
Effect of Different Lasers on Calculated P _{trap} in Quartz.....	51
CONCLUSIONS	53
REFERENCES.....	55

LIST OF TABLES

Table 1.	464 cm ⁻¹ peak of two different quartz inclusions and reference crystals using different tools (LabSpec, PeakFit, and MATLAB). The three software methods do not show significant variability in peak positions and yield comparable reproducibilities (2σ values).....	13
Table 2.	Average P _{trap} calculations ±2σ using a variety of Raman peak combinations with three different laser sources. Raman offsets were obtained using a quartz reference grain (Quartz Ref.) and a Hg-line as reference. Quartz spectra that included the Hg-line were collected on a different day, but values used to calculate Raman offsets can be considered an appropriate representation of using emission lines as an external calibration. P _{inc} calculations using 1 peak used equations from Kohn (2014). All other P _{inc} calculations were made using stRAiMAN (Angel et al., 2019) and an excel spreadsheet provided by M. Alvaro (pers. comm. to MJK, 2018). P _{trap} calculations used EosFit-Pinc (Angel et al., 2017). Low quality spectra for the red laser precluded calculations that used 206 cm ⁻¹ . Nearly all peak combinations using two distinct calculations for P _{inc} show similar P _{trap} values, except for using two peaks (128 cm ⁻¹ and 464 cm ⁻¹) with the green and red lasers, which resulted in P _{trap} of nearly 1 GPa.....	37

LIST OF FIGURES

- Figure 1. Quartz reference (Herkimer quartz) Raman spectrum. Peaks labeled as 128 cm^{-1} , 206 cm^{-1} , and 464 cm^{-1} are used in this study for reproducibility tests and Ptrap calculations.8
- Figure 2. Zircon reference (Mud Tank zircon) Raman spectrum. Peaks labeled as 975 cm^{-1} and 1008 cm^{-1} are used in this study for reproducibility tests....9
- Figure 3. Hg atomic-emission line in a Quartz reference (Herkimer quartz) Raman spectrum. Peak labeled as 484 cm^{-1} is used in this study for reproducibility tests.10
- Figure 4. Relative intensity vs. Raman 464 cm^{-1} peak position of a quartz inclusion using three different fitting tools (LabSpec, PeakFit®, and MATLAB). All three methods show similar peak positions. Peakfit® and our MATLAB code did not try to fit subsidiary peaks..... 14
- Figure 5. Illustration of how peak-to-background (P/B) ratios were calculated. Length P is the difference between maximum peak intensity and the projected value of the background under the peak center (B).15
- Figure 6. Raman Intensity vs. Raman peak positions of a quartz inclusion using the red laser. 206 cm^{-1} peak is not well-resolved and the peak fitting routine is not sufficient to use for Pinc and Ptrap calculations.17
- Figure 7. Time series of room temperature (red) and Raman shifts of the 464 cm^{-1} peak in quartz and the 1008 cm^{-1} peak in zircon using different laser sources: 532 nm = green , 442 nm = blue. Black line is the difference between these peak positions and the 484 cm^{-1} peak (a Hg-line from an external fluorescent light source). All time series show initial 0.5-1 cm^{-1} drift over the first 0.5 to 1.5 hours, long periods (several hours) of stable or slowly drifting peak position, and large and rapid shifts in peak positions (bracketing times shown by labels with arrows). Temperature commonly correlates with Raman peak positions in some periods for all four experiments, but correlations can be positive or negative. Numbers in gray circles represent such periods described in results. A) 15-hour experiment on quartz reference crystal using a 532 nm (green) laser source. B) 24-hour experiment on quartz reference crystal using a 442 nm (blue) laser source. C) 16-hour experiment on zircon reference crystal

using a 532 nm (green) laser source. D) 24-hour experiment on zircon reference crystal using a 532 nm (green) laser source.....20

- Figure 8. Peak positions vs. acquisition time (A, C) and power density (B, D) showing no significant correlations. \bar{X} = mean. m and R^2 are the slope and R^2 values of a regression of peak position vs. either power density or acquisition time. All errors are 2σ . Reproducibility of 0.1 cm^{-1} occurred during a 2-hour period. Colors of symbols and lines correspond with laser color (excitation wavelength). Circles = inclusions; squares = reference crystal. Solid lines = inclusion means; dashed lines = reference means. Data were collected on different days, so offsets between inclusion vs. reference and between green vs. blue lasers are not meaningful. A) Quartz 464 cm^{-1} peak with constant total acquisition time (30s) and varying ND filters (3-100%). B) Quartz 464 cm^{-1} peak with constant ND filter (25%) and varying total acquisition times (3 – 270s). C) Zircon 1008 cm^{-1} peak with constant total acquisition time (3s) and varying ND filters (10-100%). D) Zircon 1008 cm^{-1} peak with constant ND filter (1%) and varying total acquisition times (10 – 270s). Varying power densities and total acquisition times do not obviously affect peak positions.23
- Figure 9. Relative intensities vs. Raman wavenumbers of quartz and zircon inclusions and reference crystals. P/B represents peak to background ratios as defined in Figure 5. Colors of peaks correspond with laser color (excitation wavelength): green = 532 nm, blue = 442 nm. A) Quartz 464 cm^{-1} peak positions. B) Zircon 1008 cm^{-1} peak positions. Data were collected on different days, so offsets between inclusion vs. reference and between green vs. blue lasers are not meaningful.25
- Figure 10. Full width at half maximum (FWHM) vs. total acquisition time and power density. Colors of symbols correspond with laser color (excitation wavelength). Circles = inclusions; squares = reference crystals. A) FWHM of quartz 464 cm^{-1} peak. B) FWHM of zircon 1008 cm^{-1} peak. FWHM of Raman peaks does not vary systematically with changes in laser power or acquisition time.27
- Figure 11. Photomicrographs of zircon inclusions in a garnet host, sample ZS-B1. Pictures were taken after Raman spectral acquisition with the 442 nm (blue) laser source. Note that in panels A and B, the stage has been moved slightly so crosshair positions no longer correspond with the analytical location. A) Undamaged zircon inclusion; high power (100%) and total acquisition time of 3 seconds (s). B) Zircon inclusion with signs of damage (darkening at top of inclusion); high power (100%) and total acquisition time of 10s. C) Highly damaged zircon inclusion; high power (100%) and total acquisition time > 60s.29

- Figure 12. Time-series of characteristic peak positions of quartz and zircon inclusion and reference crystals, collected on two different days with different wavelength lasers, showing typical reproducibilities of $\sim\pm 0.2$ cm⁻¹ (2 σ) and approximately constant offsets among lasers. Colors of symbols and lines correspond with laser color (excitation wavelength). Circles = inclusion; squares = reference crystal. Solid lines = inclusion means; dashed lines = reference means. Values with errors represent mean peak positions with two sigma standard deviations. A) Quartz 464 cm⁻¹ peak. B) Zircon 1008 cm⁻¹ peak.31
- Figure 13. Time-series of the difference in the 128 cm⁻¹ peak positions and the difference in the 464 cm⁻¹ peak positions in quartz as measured using different laser sources (e.g., green vs. blue, blue vs. red, etc.). Example calculation is shown for reference and inclusion in each panel. Measurements of reference and inclusion were interspersed but are separated to facilitate comparisons. The split between reference and inclusion analyses does not represent a shift in instrument behavior. Circles = inclusions; squares = reference crystals. Yellow = 128 cm⁻¹ peaks; black = 464 cm⁻¹ peaks. A) Green vs. blue lasers. B) Blue vs. red lasers. C) Green vs. red lasers. Quartz reference has a better reproducibility than quartz inclusion, and systematic shifts occur to the peak positions for the two lasers.33
- Figure 14. Time-series of the difference in the 975 cm⁻¹ peak positions and the difference in the 1008 cm⁻¹ peak positions in zircon as measured using different laser sources. Example calculation is shown for reference and inclusion in each panel. Measurements of reference and inclusion were interspersed but are separated to facilitate comparisons. The split between reference and inclusion analyses does not represent a shift in instrument behavior. Circles = inclusions; squares = reference crystals. Yellow = 975 cm⁻¹ peaks; black = 1008 cm⁻¹ peaks. A) Green vs. blue lasers. B) Blue vs. red lasers. C) Green vs. red lasers. Zircon reference has a better reproducibility than zircon inclusion, and systematic shifts occur to the peak positions for the two lasers.34
- Figure 15. Time-series of quartz entrapment pressures (P_{trap}) using different laser sources. Colors of circles correspond with laser color (excitation wavelength). P_{trap} calculations using blue and green laser sources show similar values and variabilities (0.67 ± 0.07 GPa for blue, 0.65 ± 0.03 GPa for green). P_{trap} calculations using red laser show much higher overall P_{trap} and variability (1.00 ± 0.46 GPa).36
- Figure 16. (A) Trends and (B) correlation between quartz 464 cm⁻¹ peak and temperature at the Raman laboratory during an abrupt change in temperature at night. Blue dots = quartz peak (cm⁻¹); orange dots =

temperature (°C). ρ = correlation coefficient. Raman peak positions correlate with temperature over some intervals, but also shift abruptly...42

Figure 17.	(A) Oscillation in quartz 464 cm-1 peak position mimics oscillation in temperature with a time lag of ~4.5 minutes. (B) Correlation between quartz 464 cm-1 peak and laboratory temperature during a relatively stable period. Correlation was calculated after optimizing time offset between peak and temperature. Blue dots = quartz peak (cm-1); orange dots = temperature (°C); ρ = correlation coefficient.....43	43
Figure 18.	Negative correlation between quartz 464 cm-1 peak and laboratory temperature during a rapid change in temperature in the morning. ρ = correlation coefficient.....44	44
Figure 19.	Time-series of Hg-line (purple dots) and quartz or zircon peaks (green dots) and correlations of Hg-line with temperature (inset maps); ρ = correlation coefficient. (A) Quartz. (B) Zircon. We do not know why there are abrupt ~0.05 cm-1 shifts in the Hg-line between measurements 240 and 300 for quartz.....45	45
Figure 20.	Time-series of Hg-line (purple dots) and quartz or zircon peaks (green dots) and correlations of Hg-line with temperature (inset maps); ρ = correlation coefficient. (A) Quartz. (B) Zircon. Quartz and zircon peaks drift slowly in parallel with the Hg line, but also exhibit 0.1 to 0.4 cm-1 jumps independent of the Hg line.....46	46
Figure 21.	Raman spectra of a single zircon inclusion using different lasers. (A) blue. (B) green. (C) red. The spectra were collected sequentially with the same parameters. All three lasers show well-resolved peaks, but the red laser shows the smallest garnet intensities and highest zircon P/B, while the green laser shows the largest garnet and lowest zircon intensities. All unlabeled peaks are characteristic of zircon.51	51

LIST OF ABBREVIATIONS

P_{inc}	Inclusion Pressure
P_{trap}	Inclusion Entrapment Pressure
P-T	Pressure-Temperature
ND	Neutral Density
RMSE	Root Mean Square Error
P/B	Peak to Background
FWHM	Full Width at Half Maximum
HWHM	Half Width at Half Maximum
Ma	Millions of years ago
Myr	Millions of years
σ	Standard deviation

INTRODUCTION

Raman microspectroscopy is widely used in a variety of scientific fields such as materials science, geosciences, chemistry, and biology to identify and understand organic and inorganic molecules (e.g., Sato et al., 2001; Wahadoszamen et al., 2014). Raman microspectroscopy can be advantageous because analysis is rapid, non-invasive, and in many cases causes no damage to a sample. Raman microspectroscopy is of growing interest for geologic studies, such as to identify minerals (e.g., Korsakov et al., 2009), characterize melts and fluid inclusions (e.g., Rosasco et al., 1975; Mernagh and Wilde, 1989) and to determine pressure and temperature (P-T) of metamorphic mineral formation using mineral inclusions (e.g., Enami et al., 2007) and carbonaceous materials (e.g., Sobolev and Shatsky, 1990; Beyssac et al., 2002).

Peak position resolution of $1\text{-}2\text{ cm}^{-1}$ is sufficient for most applications of Raman microspectroscopy: nearly all studies in the Geosciences focus on either which Raman peak positions are present in a spectrum (e.g., for mineral identification), or the integrated area under certain Raman peaks (e.g., for thermometry using carbonaceous materials). However, when using mineral inclusions for elastic geothermobarometry, such as the quartz-in-garnet barometer (QuiG; Kohn, 2014), calculations are based on the peak offsets between inclusion and reference crystals. If systematic errors such as instrument calibration propagate uniformly across a spectrum, peak position offsets are retained irrespective of exact peak positions. Thus, understanding how consistently we can

measure peak positions and differences in peak positions is essential to computational accuracy.

Machine stability and spectral parameters, including laser source, power density, acquisition time, and number of gratings are the main factors that determine the precision of peak positions in Raman spectra. While research in Biology and Materials Science has sought to optimize analytical parameters (e.g., Wahadoszamen et al., 2014; Kerr et al., 2015), little effort has been published for optimizing measurements for geologic samples. Most published literature does not document in detail how analytical procedures as well as external laboratory conditions affect Raman peak positions or P-T calculations.

In this study, we quantify the stability of Raman peak positions for reference crystals and inclusions of quartz and zircon, as well as for a Hg atomic-emission line from fluorescent lights. Specifically, we report:

- Long-term stability of peak positions, using sequential ~30s measurements for up to ~30 hours.
- The effects of varying power and acquisition times on peak positions to identify whether integrated laser flux affects spectra (e.g., through laser-induced heating)
- The effects of different laser sources on peak positions to identify optimal stability, intensity, and peak-to-background ratio.

We also characterize reproducibility of calculated entrapment pressures based on repeated inclusion-standard measurements using different laser sources and computational methods. Last, we compile recommendations for data monitoring and reporting. Overall, we show that machine stability and peak drift (up to 2.5 cm^{-1}) can

affect calculated P-T conditions in natural rocks by as much as 0.35 GPa (for incautious approaches), but that optimization of analysis improves reproducibilities to $\sim\pm 0.05$ GPa.

BACKGROUND

Mineral Inclusion Elastic Barometry

Mineral inclusion elastic barometry using Raman microspectroscopy can complement classical thermobarometric methods because it does not rely on chemical equilibration of mineral assemblages. Instead, it assumes mechanical equilibrium (e.g., no differential stress or strain at the time of mineral entrapment) and relies on the P-T dependence of mineral volumes (Enami et al., 2007), i.e., each mineral's compressibility and thermal expansivity. The most commonly applied elastic barometer today is for quartz inclusions in garnet ("QuiG").

When a quartz inclusion becomes entrapped in a garnet host, the inclusion and host both experience the same P-T condition, and the void space in the garnet exactly matches the volume of the inclusion. However, as the rock cools and exhumes to the surface, the inclusion and host will attempt to achieve different volumes because they have different elastic properties (Rosenfeld and Chase, 1961). Commonly, quartz inclusions will attempt to expand against the surrounding garnet, leading to a compressed quartz lattice (negative strain or "positive pressure"). In some low-P, high-T cases, quartz inclusions will attempt to shrink relative to the surrounding garnet, leading to an expanded quartz lattice (positive strain or "negative pressure"). By correlating compressed or expanded lattices to pressure, the community commonly refers to an inclusion pressure, or " P_{inc} ", although there is no way to determine pressure directly, only strain.

Measuring the current strain on inclusions can enable us to calculate the entrapment P-T conditions of those inclusions. Angel et al. (2017) proposed a computational approach that employs the concept of an isomeke (Adams et al., 1975). An isomeke is defined as a curve in P-T space such that both the host void space and inclusion have the same change in fractional volume (Adams et al., 1975; Angel et al., 2014). Because the fractional volumes are the same, the pressure experienced by host and inclusion are the same. The theory and computational methods of Angel et al. (2017) allow entrapment pressures (“ P_{trap} ”) to be determined: the strain on an inclusion is determined by comparing its Raman spectrum to the same unstrained mineral, the strain is converted to an average P_{inc} , the isomeke is calculated for that P_{inc} , assuming elastic properties of host and inclusion, and the entrapment pressure is calculated at an assumed temperature of entrapment.

Quartz has pressure-sensitive Raman bands (Schmidt and Ziemann, 2000). Consequently, we can invert Raman spectra of characteristic peak positions in quartz to estimate the strains in the inclusion (Angel et al., 2019: stRAInMAN software). These strains can be converted to the current pressure on the quartz inclusion (P_{inc}), and P_{inc} can be inverted to obtain the entrapment pressure of the inclusion during garnet growth (Angel et al., 2014: EosFitPinc software). Thus, we can combine the differences in Raman shifts with elastic modeling to obtain the entrapment pressure of quartz inclusions during garnet growth. If we collect multiple points, we can in principle infer a P-T path (Ashley et al., 2014; Spear et al., 2014; Castro and Spear, 2016).

Reports on Measurement Protocols

Quantifying uncertainties in Raman measurements and consequently P_{trap} values requires documentation of analytical procedures as well as laboratory conditions, such as frequency of machine calibration or variations in laboratory temperature. Many studies document analytical and machine specifications (e.g., microscope model, objective, grating, spot size, etc.), spectral resolution, and the type of calibration used (e.g., Enami et al., 2007). However, few studies describe laboratory conditions, especially temperature stability, or the frequency of reference measurements. In addition, these parameters do not allow assessment of peak position reproducibility, which ultimately limits uncertainty in P_{trap} . Different approaches to calculate P_{trap} show different sensitivities to peak position uncertainty. Even relatively small shifts to peak positions can cause significant changes to calculated P_{trap} for some methods. For example, a 0.5 cm^{-1} shift to the quartz 128 cm^{-1} peak would change calculated P_{trap} by $\sim 0.07 \text{ GPa}$ using an expression from Thomas and Spear (2018). Thus, establishing norms for data collection and reporting are important for characterizing uncertainties in P-T estimates accurately and for comparing results among different laboratories.

METHODS

Samples

Our experiments were performed with reference (stress-free) crystals of Herkimer quartz and Mud Tank zircon, cut perpendicular to the c-axis. Reference crystals were cut into thin slices that were polished and separately mounted in putty, to reduce the potential of stress gradients across the crystals. For experiments performed on inclusions, we used commercially prepared and polished 100- μm thick sections. The sections contain garnets with inclusions of fully entrapped and isolated quartz and zircon. For quartz analyses, we used sample K87-21C (43.678 °N, 72.199 °W), a metapelite from west-central New Hampshire that was metamorphosed during the Acadian Orogeny (Kohn et al., 1992); for zircon inclusions, we used sample ZS-B1 (46.016 °N, 7.842 °W), a metamorphosed ophiolite from the Zermatt-Saas region, Western Alps, formed during the Alpine Orogeny and kindly provided by Dr. S Penniston-Dorland.

Naming Convention for Peak Positions

In the literature, Raman peak positions in Raman spectra are commonly referred to using a typical measured peak position, for example, the “464 cm^{-1} ,” peak in quartz (which corresponds with the A_1 vibrational mode). As shown below, peak positions for a characteristic Raman band can vary with time or between lasers by more than 1 cm^{-1} . In this study, the “464 cm^{-1} ” peak was measured at positions ranging from ~ 463 to ~ 467 cm^{-1} depending on day, time of day, or laser source, even when all other analytical conditions were fixed. For consistency, we refer to the key peaks as: 128, 206, and 464 cm^{-1} for quartz

(Figure 1), 975 and 1008 cm^{-1} for zircon (Figure 2), and 484 cm^{-1} for a characteristic Hg atomic-emission line (Figure 3) derived from fluorescent lights.

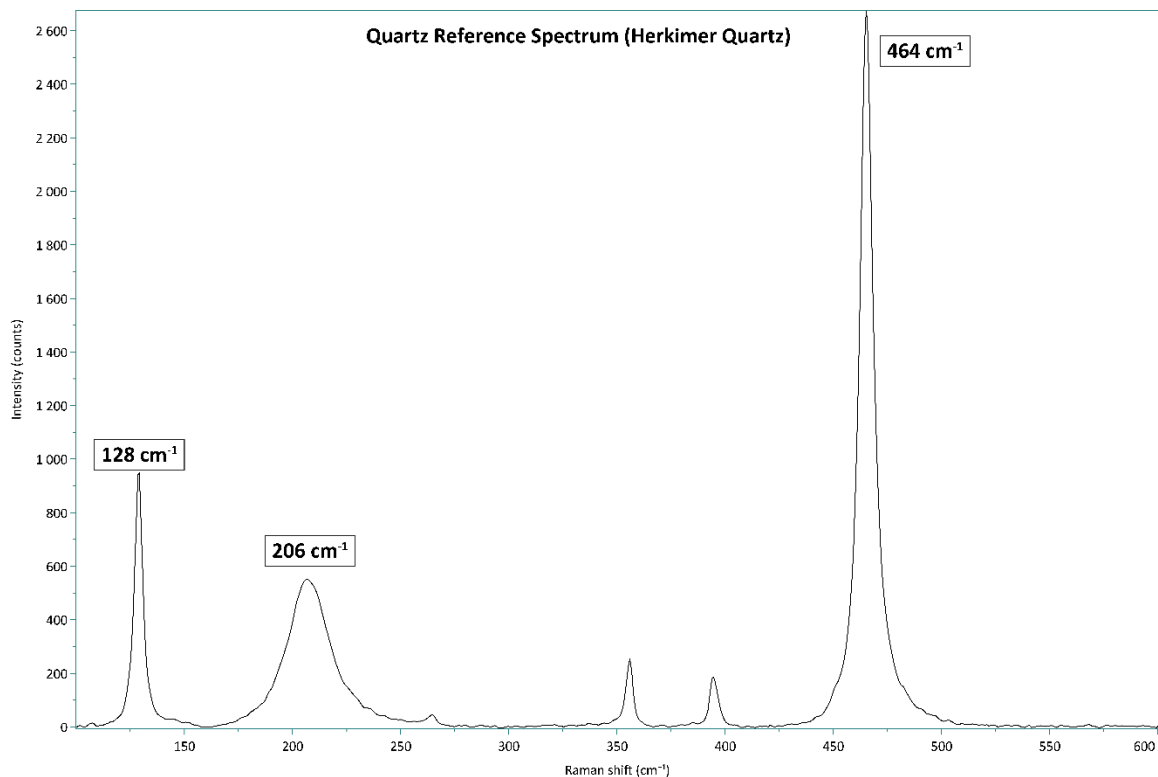


Figure 1. Quartz reference (Herkimer quartz) Raman spectrum. Peaks labeled as 128 cm^{-1} , 206 cm^{-1} , and 464 cm^{-1} are used in this study for reproducibility tests and Ptrap calculations.

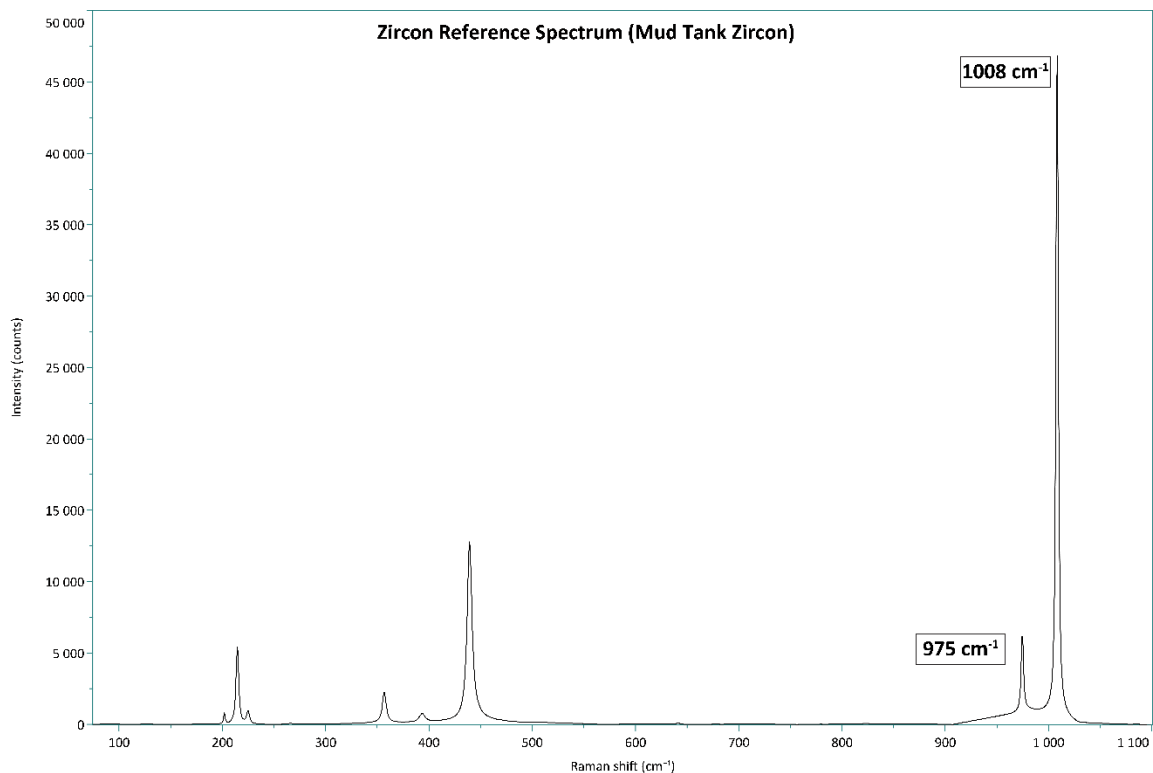


Figure 2. Zircon reference (Mud Tank zircon) Raman spectrum. Peaks labeled as 975 cm⁻¹ and 1008 cm⁻¹ are used in this study for reproducibility tests.

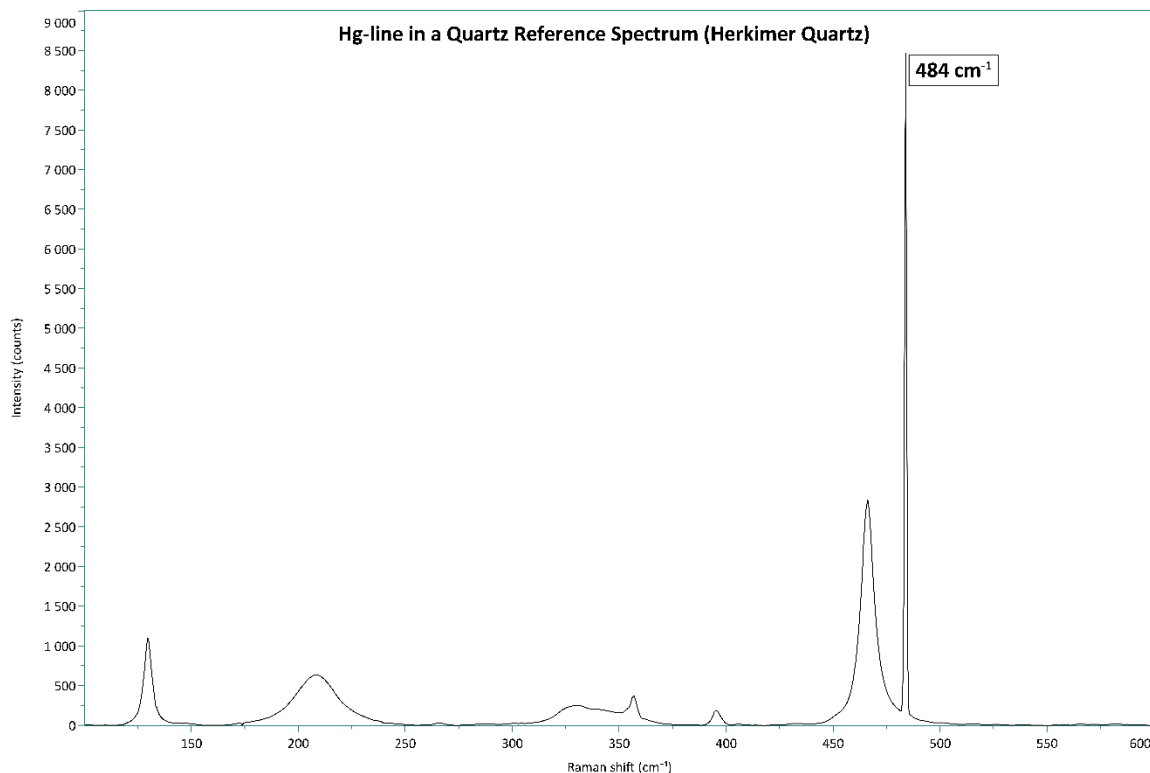


Figure 3. Hg atomic-emission line in a Quartz reference (Herkimer quartz) Raman spectrum. Peak labeled as 484 cm⁻¹ is used in this study for reproducibility tests.

Raman Measurements

For Raman spectral collection, we used a Horiba Scientific LabRAM HR Evolution at Boise State University. Experiments were performed with three different excitation laser sources: 632.8 nm He:Ne (red wavelength) with an output of about 17mW, 532 nm doubled Nd:YAG (green wavelength) with an output power of about 50 mW, and 442 nm He:Cd (blue wavelength) with an output of about 120 mW. Output powers were not measured directly and were lower in some measurements (as determined from lower count rates), likely because of drift in alignment. The Raman system is coupled with a thermoelectrically cooled charge-coupled device (CCD) detector (800-mm focal length) with a holographic diffraction grating resolution of 1,800 line/mm and a

fixed 100- μm aperture size, which gives a confocal (vertical) resolution of roughly 3-4 μm and a spectral resolution of 0.3, 0.5, and 0.8 cm^{-1} for the red, green, and blue lasers, respectively. We monitored the internal calibration at the beginning of each day with a mounted Si wafer, and we used quartz and zircon reference crystals to check the stability of the system throughout the day. We also monitored laser stability over hours of Raman spectral collection using a Hg atomic-emission line, derived from a fluorescent light. For all experiments, we used an Olympus 100x objective, which had the highest spatial resolution (less than 1 μm in X and Y) in comparison to the other available objectives, with a 0.90 numerical aperture and 210 μm working distance. The spectral range used for analyses was between 100 and 600 cm^{-1} for quartz and 75-1100 cm^{-1} for zircon. We chose the specified ranges for three reasons: (1) they have the most relevant peaks for our experiments, (2) they cover almost the entire quartz and zircon spectra when excited in the three different wavelengths, and (3) they allow us to look at the Hg-line (484 cm^{-1}) when using the green laser. Influence of laser power and laser drift were evaluated in reference peaks for the 128, 206, and 464 cm^{-1} peaks for quartz, and the 1008 cm^{-1} peak zircon.

Raman spectra used for tests of drift and power density were collected over a small region of a reference grain (about 0.5 by 0.5 μm) with either DuoScan™ imaging or the Marzhauser stage. We used a “scan” rather than point-by-point mode in the software because it was easiest to automate the instrument over periods of hours to tens of hours. We used Neutral Density (ND) filters ranging from 1 to 100%. For drift tests, the total acquisition time for each analysis was approximately 30 seconds (10 seconds per acquisition and 3 accumulations), and for power density tests, from 3 seconds up to 270

seconds. Spectra collected at lower power densities had longer acquisition times. For spectra containing the 484 cm^{-1} Hg-line, we used an external light source that was placed adjacent to the microscope. We note that use of a larger microscope objective can allow overhead light to leak into the instrument, providing another source of the 484 cm^{-1} Hg-line for fluorescent lighting.

Peak Fitting

Raman peaks were fitted using an in-house MATLAB® code which was based on a non-linear least squares curve-fitting method. We used a representative high-count rate spectrum as reference to optimize the fitting process and then applied the fitting routine to unknowns. Each Raman peak was fitted using either Gaussian, Lorentzian, or the sum of both functions over specific spectral ranges. The processes in fitting optimization include: (1) using an open source function (“baseline”) that performs an automated baseline correction of Raman spectra (Al-Rumaithi, 2020); (2) clipping the desired spectral range from the total spectrum and using this range to define the initial parameters for the fitting routine, which are peak intensity, location, and width. Initial peak intensity was assigned to the highest value on the spectrum; initial peak location was assigned to the nominal peak position expected in that spectral range (e.g., 128 , 206 , and 464 cm^{-1} for quartz; 1008 cm^{-1} for zircon); peak width was assigned as the half width at half maximum (HWHM); (3) using the Curve Fitting toolbox application from MATLAB® along with the initial parameters to generate three different functions: a) Gaussian, b) Lorentzian, and c) sum of Gaussian and Lorentzian. Each function returned estimated peak positions within the specified range and the root mean square error (RMSE) of the fitting. All peak positions reported here correspond with the function with the lowest RMSE.

To confirm the precision of the MATLAB® code, we compared our fits with two other commercial software packages – LabSpec 6 (native software for our microscope) and PeakFit®. Table 1 displays peak positions of two different quartz inclusions and reference crystals using the three different tools, and Figure 4 shows the fitted curves for quartz inclusion 1. Differences in fits are at or below our level of spot-to-spot reproducibility, with a variation of approximately $\pm 0.02 \text{ cm}^{-1}$. We prefer our MATLAB® code because it is highly efficient (up to 95 spectral text files per minute).

Table 1. 464 cm^{-1} peak of two different quartz inclusions and reference crystals using different tools (LabSpec, PeakFit, and MATLAB). The three software methods do not show significant variability in peak positions and yield comparable reproducibilities (2σ values).

464.00 (cm^{-1})	LabSpec	PeakFit	MATLAB	S.D (2σ)
Quartz Inclusion 1	465.26	465.27	465.25	0.02
Quartz Inclusion 2	465.15	465.16	465.13	0.03
Quartz Reference 1	465.34	465.35	465.35	0.01
Quartz Reference 2	465.45	465.46	465.44	0.02

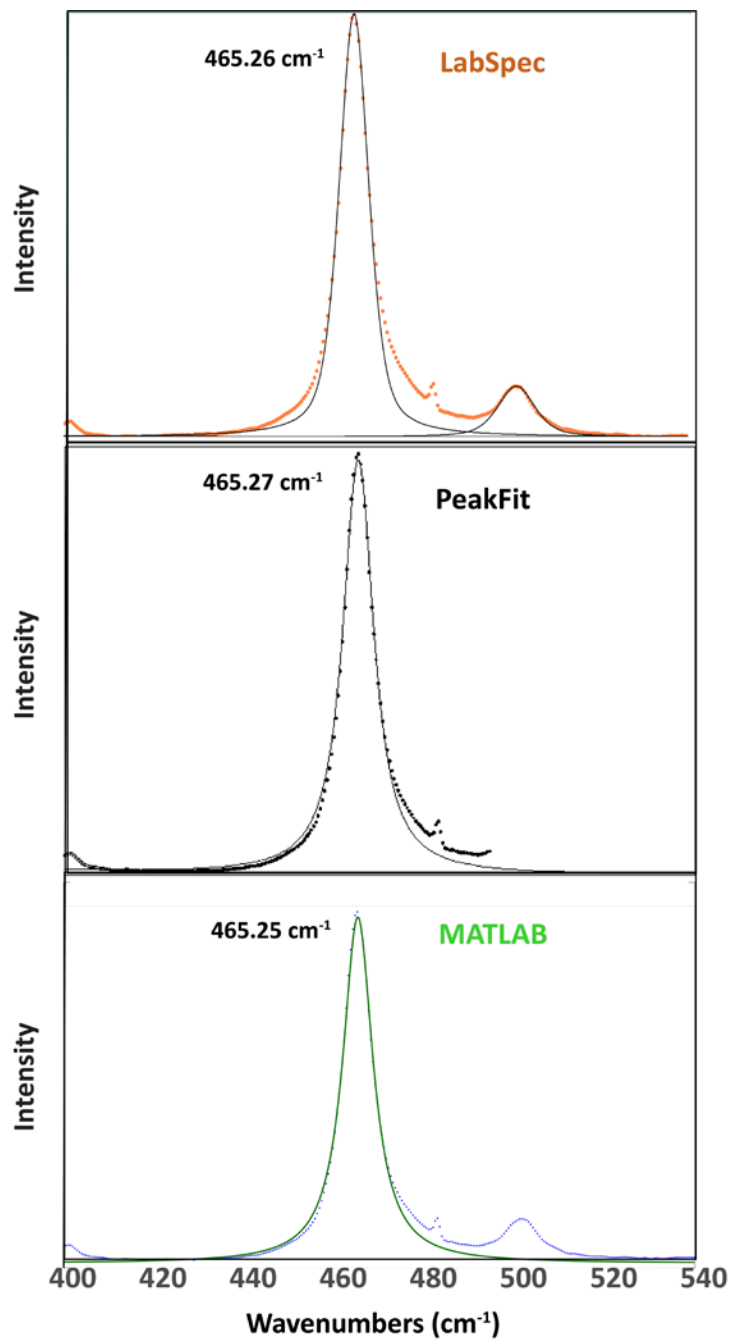


Figure 4. Relative intensity vs. Raman 464 cm⁻¹ peak position of a quartz inclusion using three different fitting tools (LabSpec, PeakFit®, and MATLAB). All three methods show similar peak positions. Peakfit® and our MATLAB code did not try to fit subsidiary peaks.

Peak to Background Ratio Calculations

Peak to background (P/B) ratios can help assess laser stability and performance in a system, so we investigated whether P/B ratios changed with changes in acquisition times and power densities. We calculated P/B ratios based on the difference between maximum peak intensity and the projected value of the background under the peak center (Figure 5).

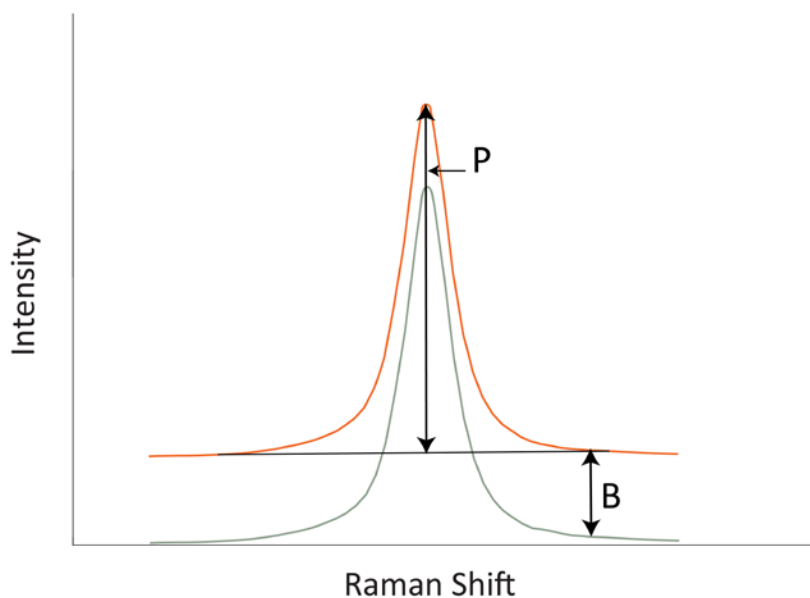


Figure 5. Illustration of how peak-to-background (P/B) ratios were calculated. Length P is the difference between maximum peak intensity and the projected value of the background under the peak center (B).

Temperature Measurements

Laboratory temperature was recorded every minute with a CR800 Campbell Scientific datalogger and a Campbell Scientific CS215 temperature and relative humidity probe, with an accuracy of ± 0.3 °C at 25 °C. The precision of our temperature

measurements was ± 0.01 °C 2σ , as determined from the reproducibility of measurements collected over short periods of time (tens of minutes). The temperature probe was approximately 80 cm away from the CCD detector, recording the temperature of the laboratory room. Because each Raman spectrum had a total acquisition time of approximately 30 seconds, the temperature and Raman records are offset. Consequently, we used a MATLAB 1-D, cubic spline, interpolation built-in function (“interp1”) to correlate temperature and acquisition time.

Laser Source Comparisons on Quartz and Zircon

Three different laser sources (blue, green, and red) were used to collect Raman spectra of the same quartz and zircon inclusion and reference crystals with fixed total acquisition time and power density of ~30 seconds and 50%, respectively. Measurements for quartz were collected on a different day than zircon. Quartz Raman spectra were collected by alternating between inclusion and reference measurements in a 4-hour period (5-hour period for zircon), with a total of 19 spectra (20 spectra for zircon) for inclusion and reference crystals using each laser source.

Entrapment Pressure (P_{trap}) Calculations

We calculated P_{trap} for a quartz inclusion in garnet using the peak offsets measured with the three different laser sources. These calculations check the reproducibility of calculated P_{trap} , assess potential differences in calculated P_{trap} using different laser sources, and permit quantitative comparison to the results obtained using thermodynamics (Kohn et al., 1992). We used a quartz inclusion from the core of a garnet host, approximately 45 μm from the surface of the thick section. To calculate P_{trap} values, we used our MATLAB code to quantify peak shifts and used the software stRAinMAN

(Angel et al., 2019) to calculate the strains in the inclusion with the 128, 206 and 464 modes (with the exception of the red laser, where the 206 peaks were unresolvable due to low spectral quality; see Figure 6). We then converted strains to average inclusion pressure (P_{inc}) based on methods outlined in Gonzalez et al. (2019) using an Excel spreadsheet kindly provided by M. Alvaro (pers. comm. to MJK, 2018). Lastly, we determined P_{trap} values using EosFit-Pinc software (Angel et al., 2017). In addition to the methods used to calculate P_{trap} values described above, we used equations from Kohn (2014) and Thomas and Spear (2018) to calculate P_{inc} values with either the 128 or 206 or 464 peak; we then used the EosFit-Pinc software to calculate P_{trap} . We tested a variety of peak combinations, including using 1, 2, or 3 peaks, to calculate P_{inc} and P_{trap} values. These calculations were based on the Raman peak offsets for the inclusion vs. either a quartz reference crystal or a Hg-line spectrum. Note that quartz inclusion and reference measurements were collected on the same day; however, the Hg-line spectra were collected on a different day. All data used to calculate the offsets were collected during periods of machine stability.

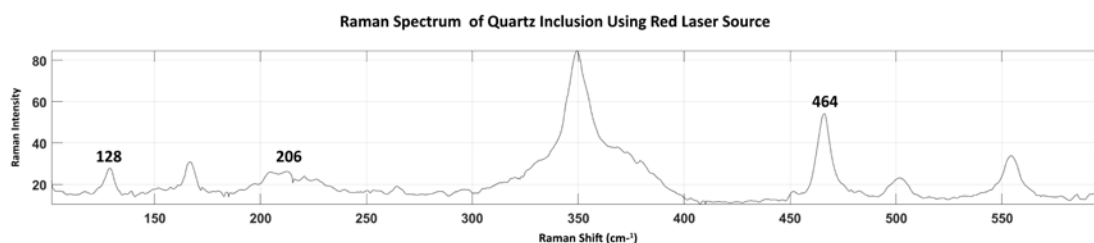


Figure 6. Raman Intensity vs. Raman peak positions of a quartz inclusion using the red laser. 206 cm⁻¹ peak is not well-resolved and the peak fitting routine is not sufficient to use for P_{inc} and P_{trap} calculations.

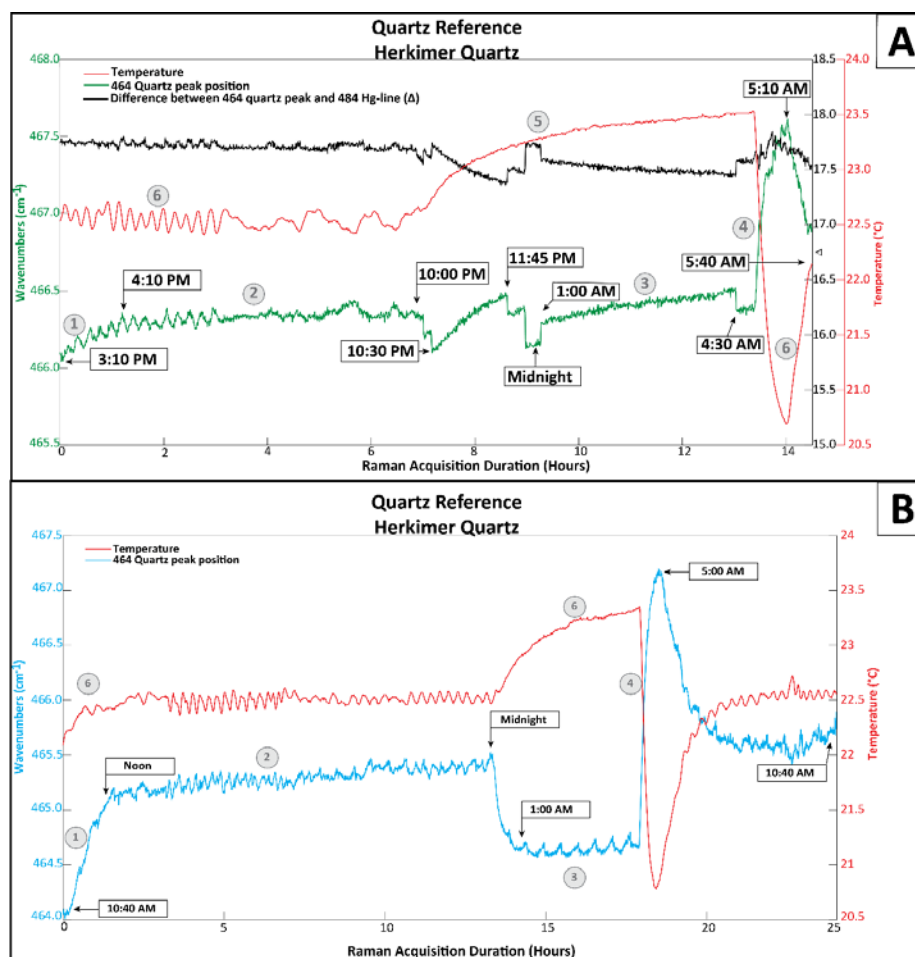
RESULTS

Peak Drift

Laser stabilization and changes in laboratory conditions can potentially influence the precision of Raman spectral measurements. Our day-long stability experiments using the green and blue lasers show several recurring features, listed here and illustrated in Figure 7:

1. Initial Drift. Within the first ~1 hour after turning on both laser sources, peak positions drift by as much as $\sim 1 \text{ cm}^{-1}$ for both quartz and zircon (hours 0 to 1, Figures 7A-D).
2. Stabilization. After ~1 hour, all Raman spectra show a period up to 5 hours of very slow drift ($0.01\text{-}0.02 \text{ cm}^{-1}/\text{hr}$; hours 1 to 6, Figures 7A-D).
3. Other Slow Drift Periods. After the first ~5 hours, other periods up to several hours long show slow drift of $<\sim 0.05 \text{ cm}^{-1}/\text{hr}$ (e.g., hours 9 to 13, Figure 7A; hours 14-18, Figure 7B, etc.). These periods are not necessarily consistent from day to day.
4. Abrupt Changes. Changes of 0.1 to $>1 \text{ cm}^{-1}$ occur at rates ranging from ~ 0.7 to $>5 \text{ cm}^{-1}/\text{hour}$ (white labels, Figure 7). The timing of shifts is not always consistent from day to day, except at $\sim 5:00$ AM local time, when the air handling system for the building switches from “night mode” to “day mode.” Many shifts also occur near midnight.

5. Shifts to Peak Offsets Relative to External 484 cm^{-1} Reference. The difference in the peak position of one of the mineral reference peaks (464 cm^{-1} for quartz, 1008 cm^{-1} for zircon) relative to the 484 cm^{-1} Hg-line also shows slow drift and abrupt changes, but the abrupt changes are much smaller in amplitude ($<\sim 0.4\text{ cm}^{-1}$) than in absolute peak position.
6. Temperature Correlations. Peak positions broadly correlate negatively with temperature, but the correlation is not consistent (e.g., at ~ 15 hours, Figure 7B) and sometimes correlations are positive (e.g., at ~ 15 hours, Figure 7D). Some rapid peak position shifts occur while temperature is changing gradually (e.g., between 7 and 10 hours, Figure 7A; at ~ 5 hours, Figure 7C).



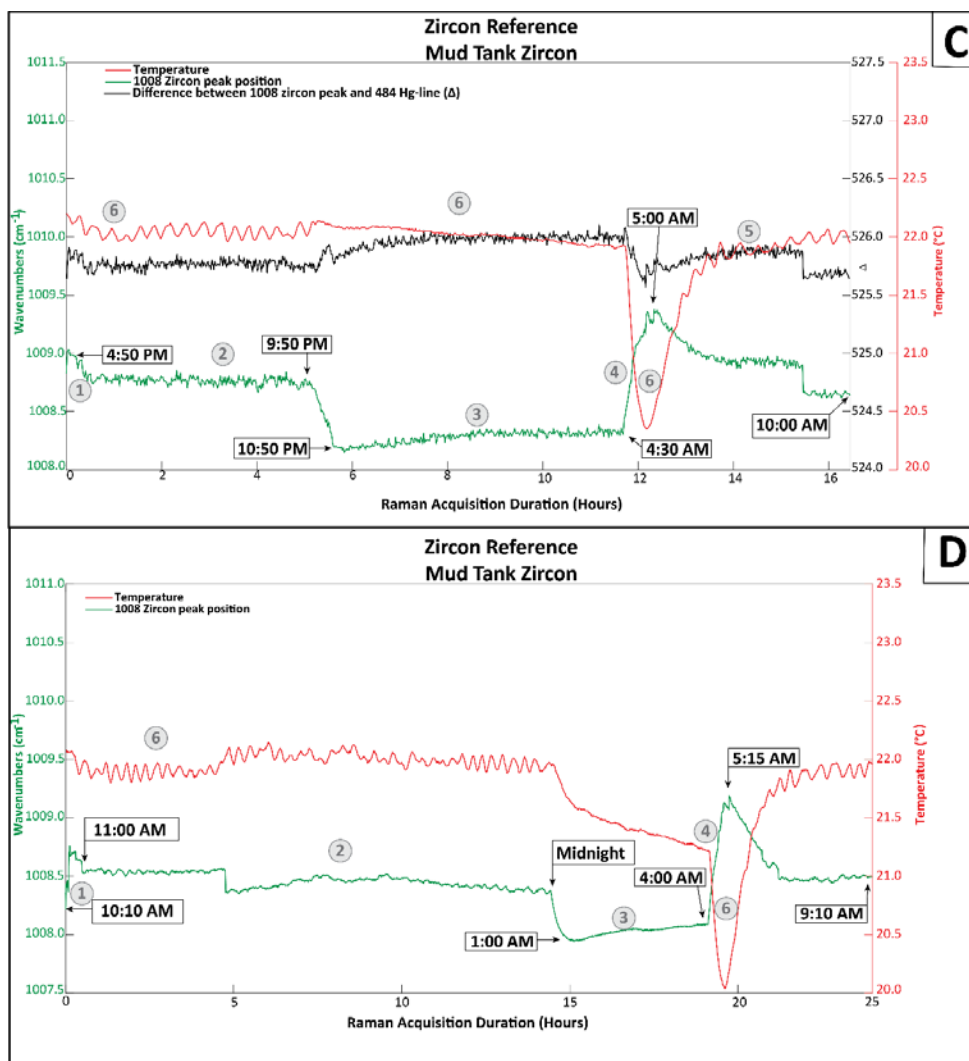
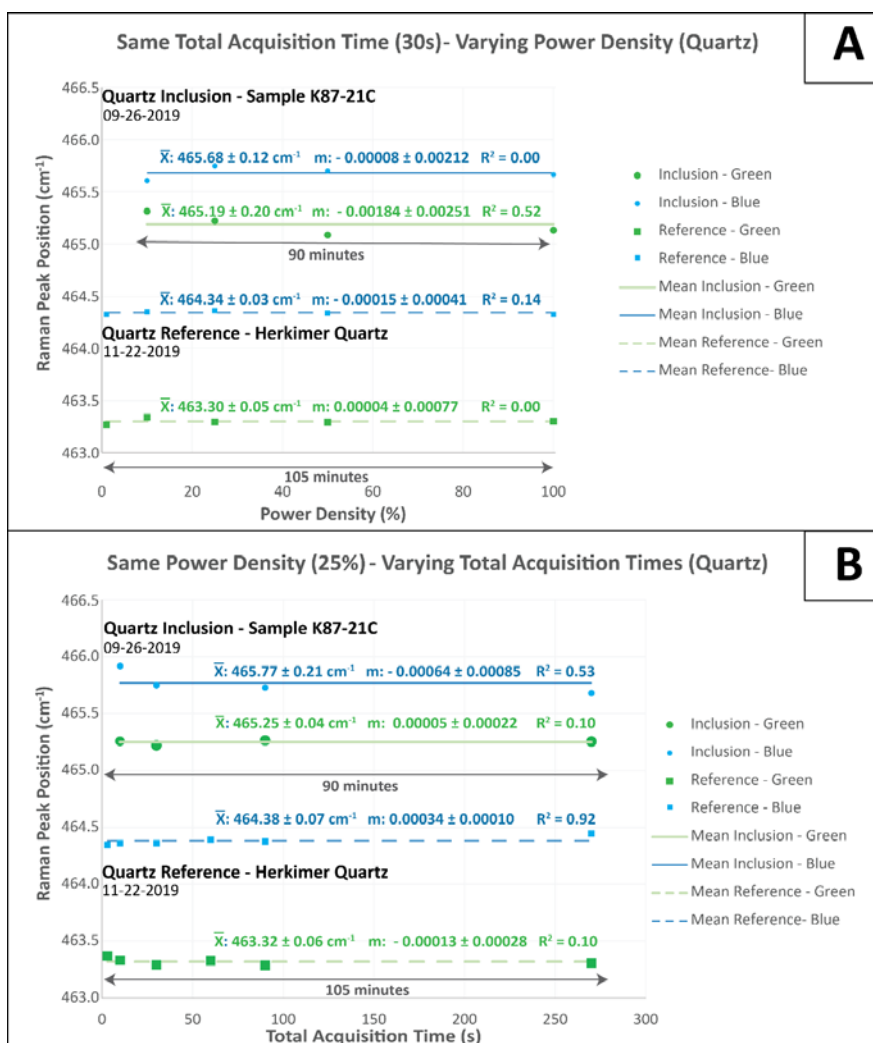


Figure 7. Time series of room temperature (red) and Raman shifts of the 464 cm^{-1} peak in quartz and the 1008 cm^{-1} peak in zircon using different laser sources: 532 nm = green, 442 nm = blue. Black line is the difference between these peak positions and the 484 cm^{-1} peak (a Hg-line from an external fluorescent light source). All time series show initial $0.5\text{--}1\text{ cm}^{-1}$ drift over the first 0.5 to 1.5 hours, long periods (several hours) of stable or slowly drifting peak position, and large and rapid shifts in peak positions (bracketing times shown by labels with arrows). Temperature commonly correlates with Raman peak positions in some periods for all four experiments, but correlations can be positive or negative. Numbers in gray circles represent such periods described in results. A) 15-hour experiment on quartz reference crystal using a 532 nm (green) laser source. B) 24-hour experiment on quartz reference crystal using a 442 nm (blue) laser source. C) 16-hour experiment on zircon reference crystal using a 532 nm (green) laser source. D) 24-hour experiment on zircon reference crystal using a 532 nm (green) laser source.

Effects of Power Density and Total Acquisition Time

Changing power density and total acquisition time in Raman spectral collection can help identify power absorption and heating that could alter Raman peak positions and calculated P_{trap} . Very generally, increases in temperature cause downward shifts in peak positions, and broadening of the full width at half maximum (FWHM) values of peaks. Our measurements show no trends in peak position vs. either power density or acquisition time (Figure 8). For both blue and green lasers, during a 1- to 2-hour experiment, peak position reproducibilities range from ± 0.04 to $\pm 0.21 \text{ cm}^{-1} 2\sigma$ for quartz inclusions, and ± 0.03 to $\pm 0.07 \text{ cm}^{-1} 2\sigma$ for the reference crystal (Figures 8A and 8B). For zircon, peak position reproducibilities range from ± 0.09 to $\pm 0.22 \text{ cm}^{-1} 2\sigma$ for inclusions, and from ± 0.07 to $\pm 0.17 \text{ cm}^{-1} 2\sigma$ for the reference crystal (Figures 8C and 8D). In figure 8, slopes of nearly all the data are not significantly different from 0.0, indicating that dependencies of peak position on power density and acquisition time are not statistically significant. The variation in peak positions as measured for a single laser under different power densities and acquisition times is comparable to the reproducibility that we observe for multiple analyses collected on the same material with different parameters. Furthermore, P/B ratios are relatively constant with varying powers and acquisition times (Figure 9). Peak width (FWHM) shows no correlation between increasing power density or acquisition time (Figure 10). There is more variation in FWHM with inclusions than with reference crystals. FWHM values within quartz and zircon inclusions vary between 0.5 and 2.3 cm^{-1} , and these variations are unrelated to the laser source used. For reference crystals, FWHM values do not vary when power densities increase using the blue laser source; however, with the green laser, changing both power density and total acquisition time caused the

FWHM values to vary from 0.5 to 1.9 cm^{-1} . Our data show that varying density powers and total acquisition times do not influence the values of peak positions as long as the inclusion or reference crystal does not show signs of laser-induced damage.



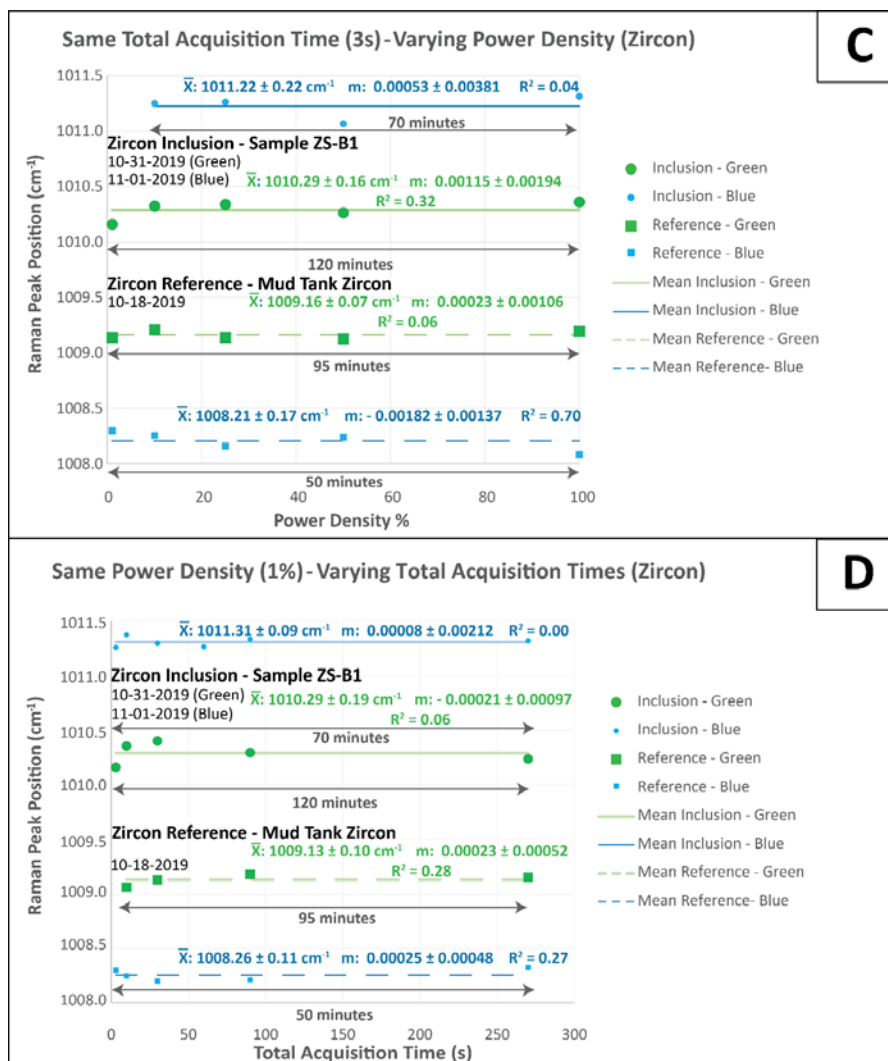
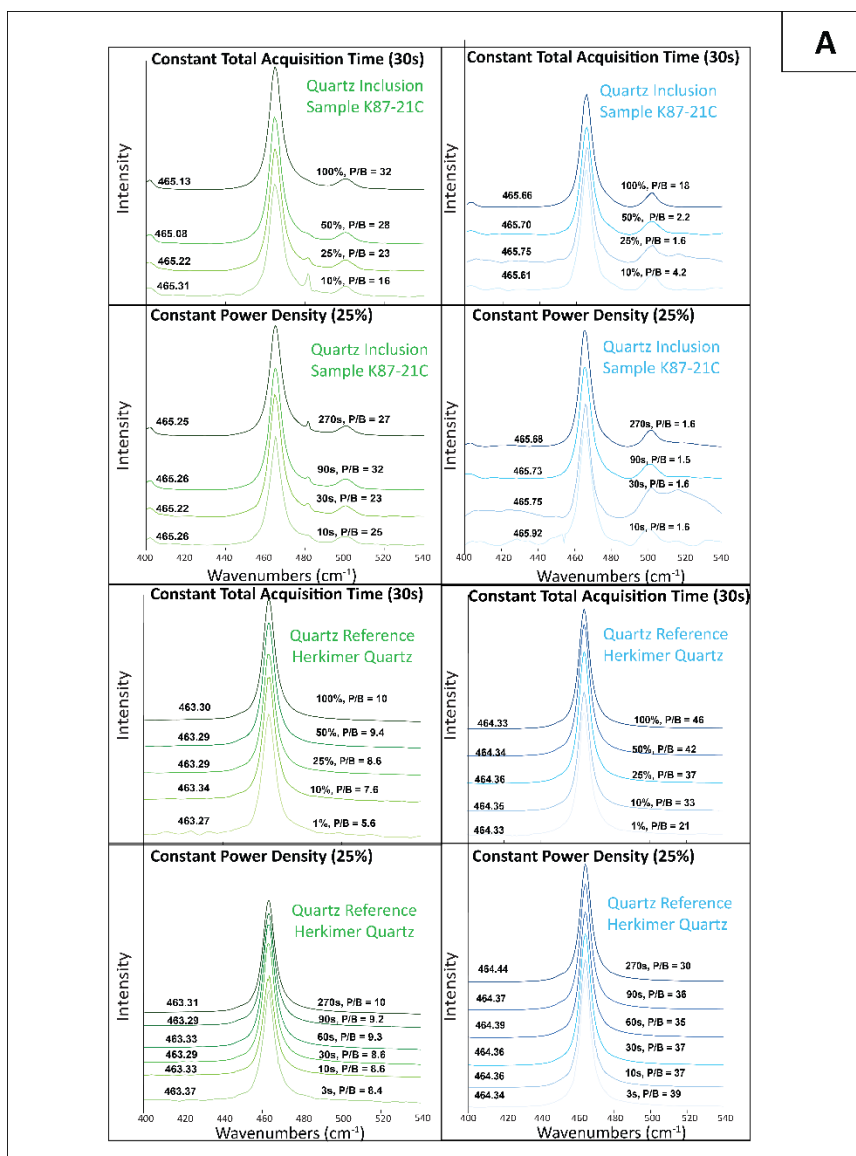


Figure 8. Peak positions vs. acquisition time (A, C) and power density (B, D) showing no significant correlations. \bar{X} = mean. m and R^2 are the slope and R^2 values of a regression of peak position vs. either power density or acquisition time. All errors are 2σ . Reproducibility of 0.1 cm^{-1} occurred during a 2-hour period. Colors of symbols and lines correspond with laser color (excitation wavelength). Circles = inclusions; squares = reference crystal. Solid lines = inclusion means; dashed lines = reference means. Data were collected on different days, so offsets between inclusion vs. reference and between green vs. blue lasers are not meaningful. A) Quartz 464 cm^{-1} peak with constant total acquisition time (30s) and varying ND filters (3-100%). B) Quartz 464 cm^{-1} peak with constant ND filter (25%) and varying total acquisition times (3 – 270s). C) Zircon 1008 cm^{-1} peak with constant total acquisition time (3s) and varying ND filters (10-100%). D) Zircon 1008 cm^{-1} peak with constant ND filter (1%) and varying total acquisition times (10 – 270s). Varying power densities and total acquisition times do not obviously affect peak positions.

A



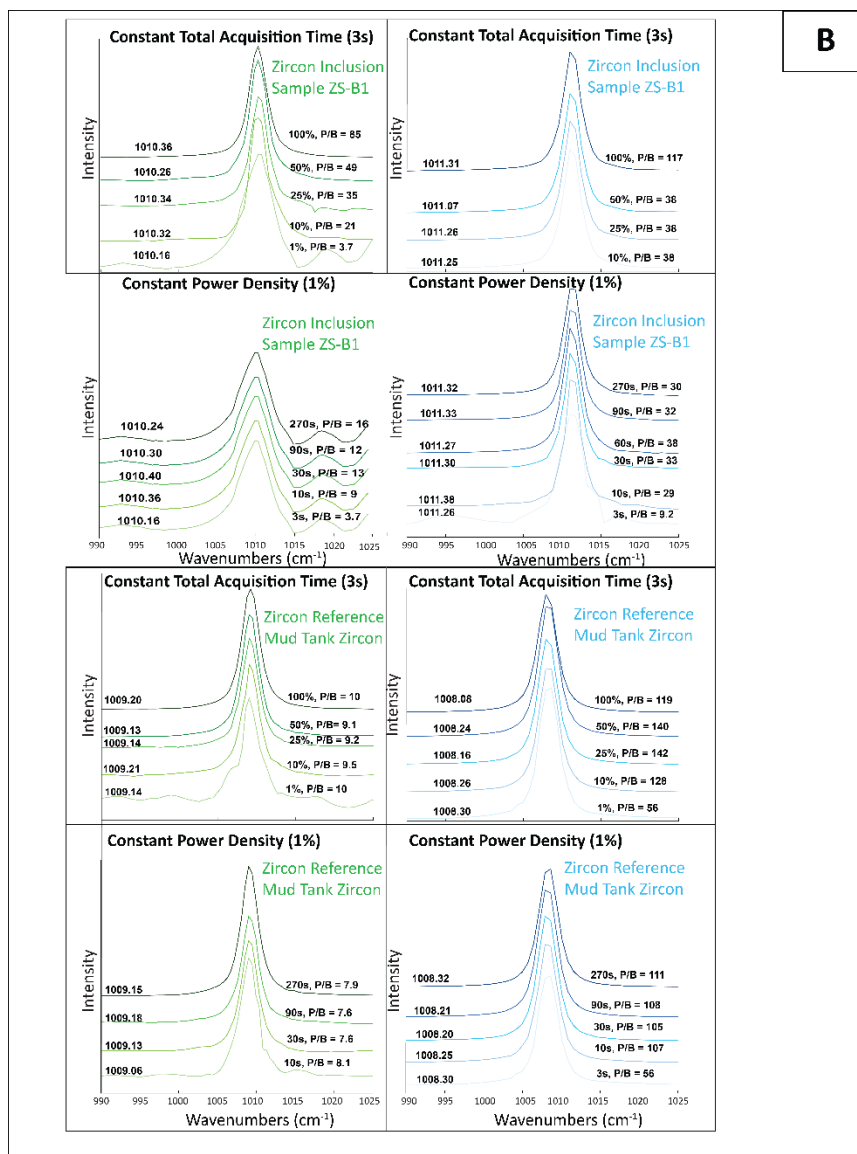
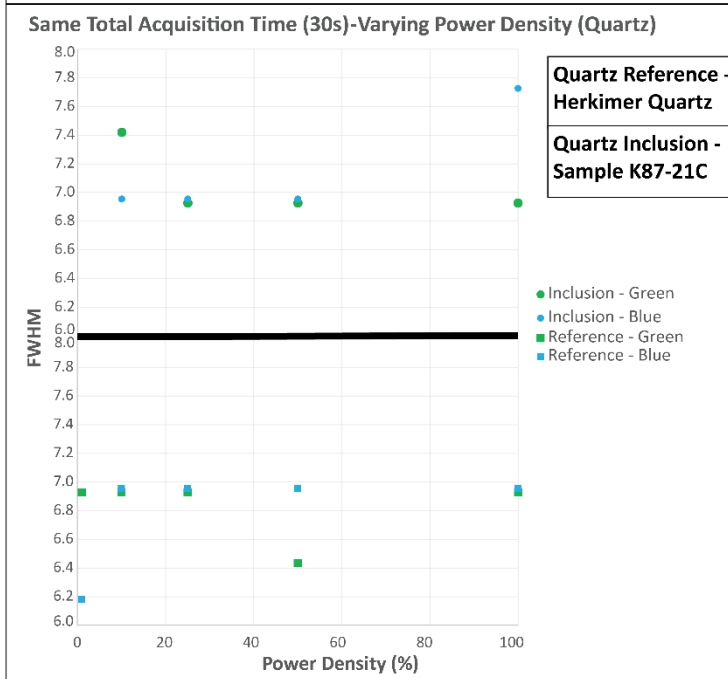
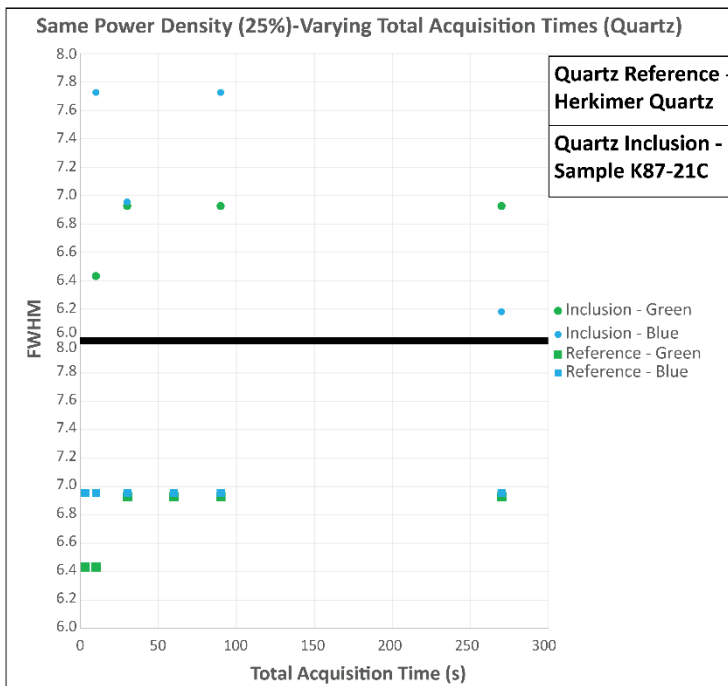


Figure 9. Relative intensities vs. Raman wavenumbers of quartz and zircon inclusions and reference crystals. P/B represents peak to background ratios as defined in Figure 5. Colors of peaks correspond with laser color (excitation wavelength): green = 532 nm, blue = 442 nm. A) Quartz 464 cm⁻¹ peak positions. B) Zircon 1008 cm⁻¹ peak positions. Data were collected on different days, so offsets between inclusion vs. reference and between green vs. blue lasers are not meaningful.

A



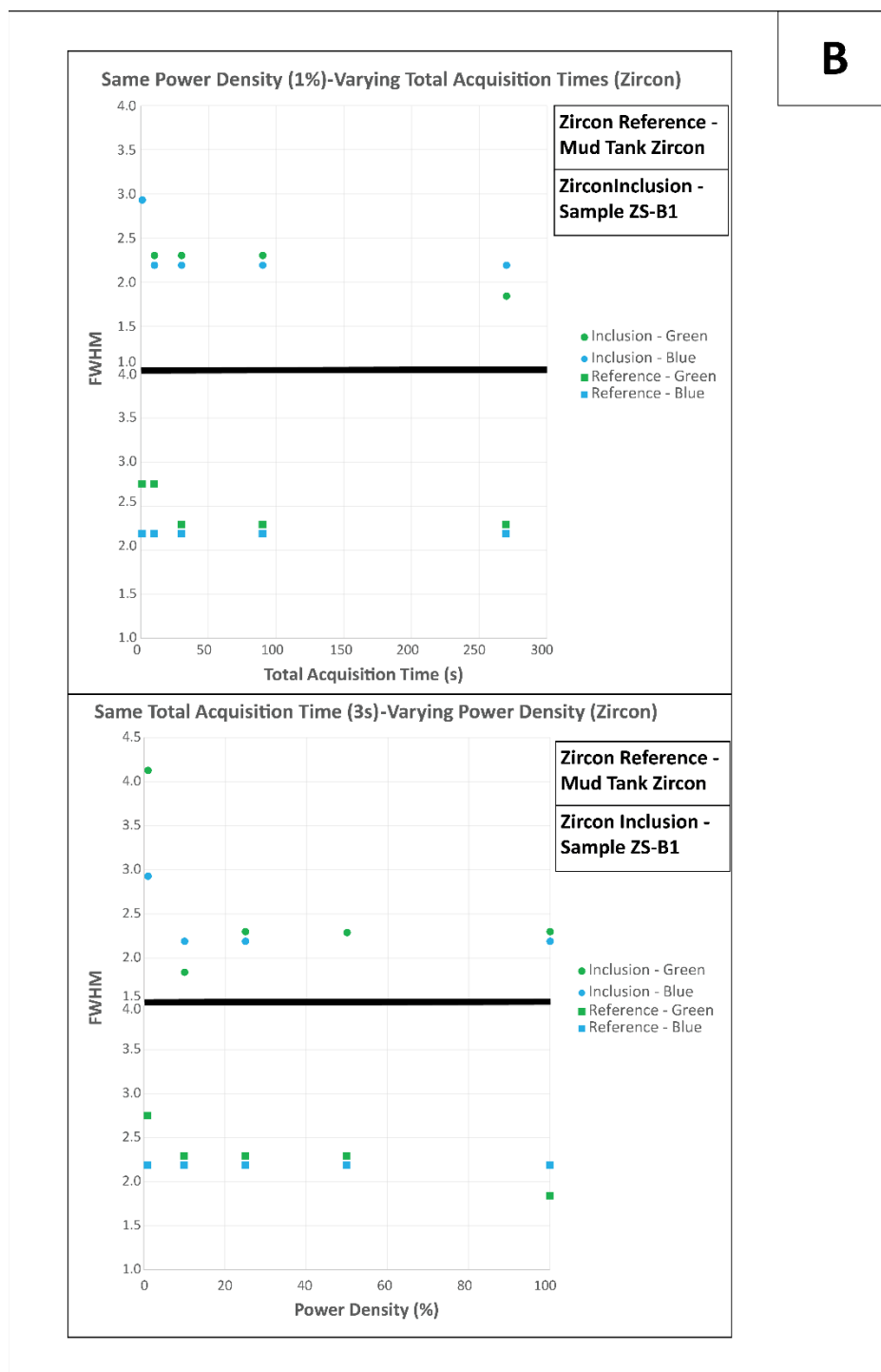


Figure 10. Full width at half maximum (FWHM) vs. total acquisition time and power density. Colors of symbols correspond with laser color (excitation wavelength). Circles = inclusions; squares = reference crystals. A) FWHM of quartz 464 cm^{-1} peak. B) FWHM of zircon 1008 cm^{-1} peak. FWHM of Raman peaks does not vary systematically with changes in laser power or acquisition time.

Zircon Damage Using Blue Excitation Wavelength

In the process of collecting Raman spectra of zircon inclusions with the blue laser at varying power densities, massive damage occurred to a zircon inclusion. Figure 11 shows zircon inclusions from sample ZS-B1 at approximately 50 μm below the garnet surface in different stages of damage. Use of a ND filter of 100% and a total acquisition time of 3 seconds did not visibly damage the inclusion (Figure 11A). Increasing acquisition time to 10s (with a ND filter of 100%) produced signs of damage in the inclusion, namely a dark spot in the top left of the inclusion (Figure 11B). A further increase to an acquisition time of about a minute (with a ND filter of 100%) resulted in massive damage to the inclusion and surrounding garnet (Figure 11C). We were not able to damage zircon inclusions visibly using the green laser source, even when reproducing the same experimental conditions. A few months later we repeated the experiment of extending acquisition time to test the potential for the laser to damage an inclusion, and we failed to reproduce these results and damage inclusions. Explanations for differences in behavior on different days are considered in the discussion below.

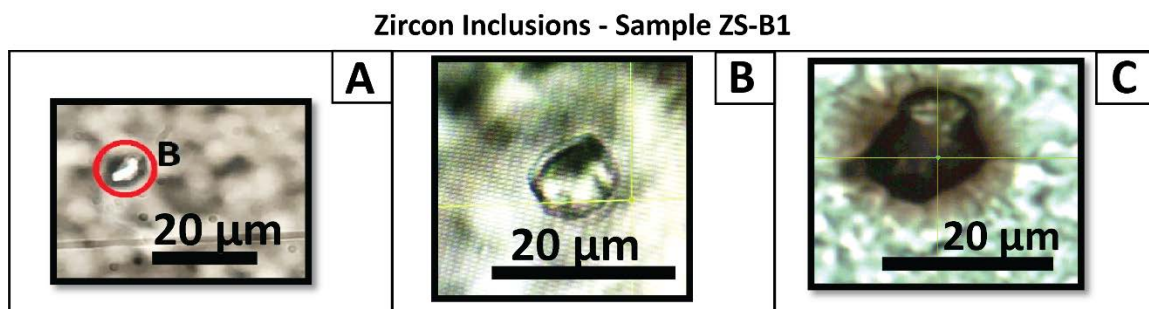


Figure 11. Photomicrographs of zircon inclusions in a garnet host, sample ZS-B1. Pictures were taken after Raman spectral acquisition with the 442 nm (blue) laser source. Note that in panels A and B, the stage has been moved slightly so crosshair positions no longer correspond with the analytical location. **A)** Undamaged zircon inclusion; high power (100%) and total acquisition time of 3 seconds (s). **B)** Zircon inclusion with signs of damage (darkening at top of inclusion); high power (100%) and total acquisition time of 10s. **C)** Highly damaged zircon inclusion; high power (100%) and total acquisition time > 60s.

Peak to Background Ratios Using Blue Laser

Blue lasers are less commonly used than red and green lasers, so providing more details about these results are warranted. The blue laser gives higher Raman intensity counts than the green laser source on zircon crystals. Using the blue laser source yielded higher P/B ratios for both quartz and zircon reference crystals and zircon inclusions, but not for quartz inclusions. Depending on the power density and acquisition time used, the Raman intensity counts using the blue laser were up to 20 times higher than intensity counts using the green laser. Using the blue laser, we obtained a high-resolution spectrum with a total acquisition time of 3 seconds and P/B ratio of 56 (Figure 9B). In comparison, when using the same parameters but changing the laser source to green, we obtained a P/B ratio of ~8. These results confirm that the blue laser source gives high Raman intensity counts with very low background noise.

Laser Source Comparisons

Reproducibilities

Both quartz and zircon inclusions and reference crystals show similar reproducibility of $\sim 0.2 \text{ cm}^{-1} 2\sigma$ for the 464 cm^{-1} and 1008 cm^{-1} peaks, except for the measurements made with the red laser on quartz (0.1 cm^{-1}). Quartz measurements using the red laser show better reproducibility over the 4-hour experiment in comparison to the green and blue lasers (Figure 12). For quartz, we obtained a variance of 0.08 and $0.20 \text{ cm}^{-1} 2\sigma$ for reference crystal analyses and inclusion analyses, respectively (Figure 12A). For zircon, the resulting variances were 0.11 and $0.17 \text{ cm}^{-1} 2\sigma$ for reference crystal analyses and inclusion analyses, respectively (Figure 12B). Oscillations in peak positions occurred throughout the experiment and reached amplitudes as high as 0.45 cm^{-1} ; however, the oscillation is more attenuated for reference spectra (approximately 0.1 cm^{-1}).

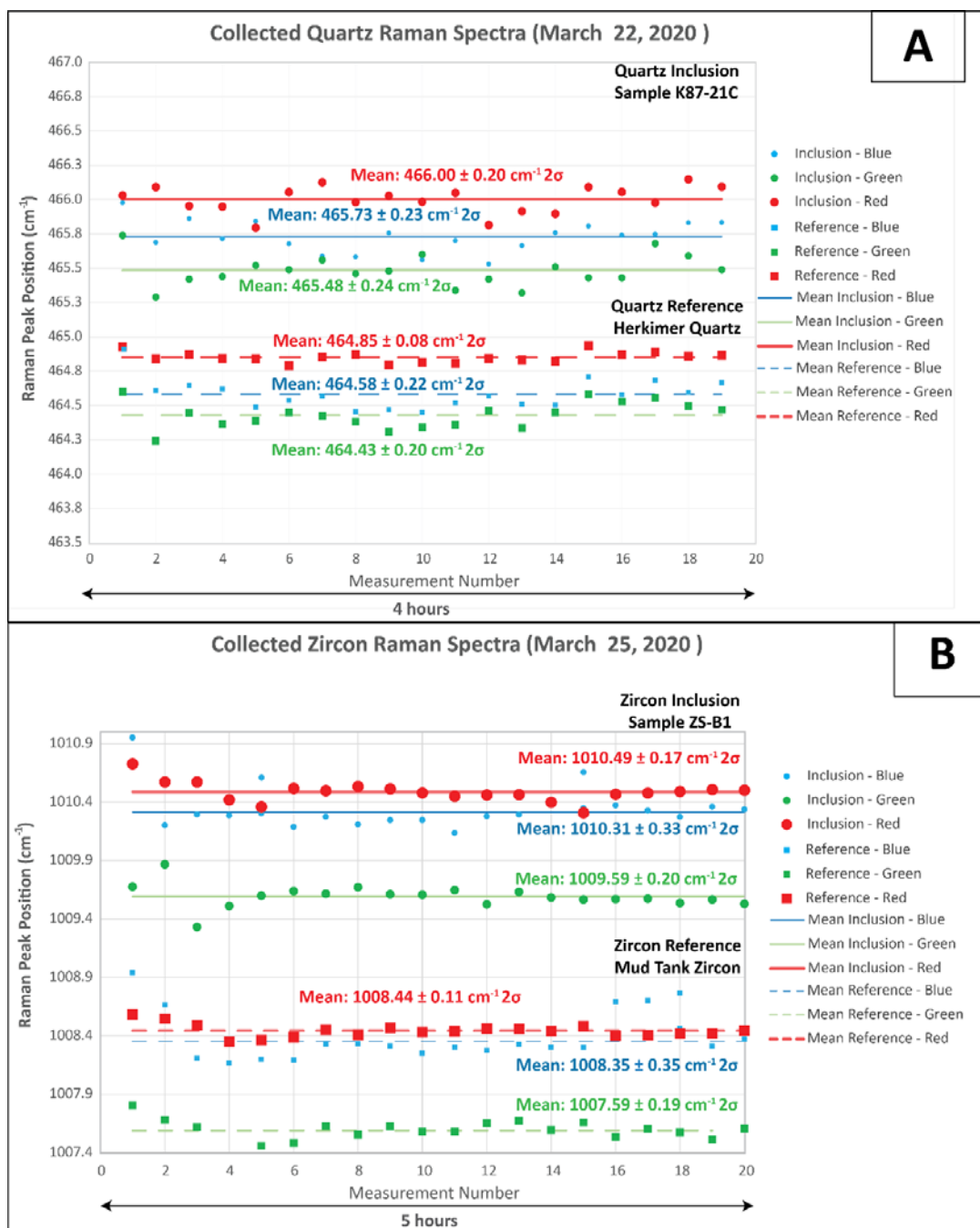


Figure 12. Time-series of characteristic peak positions of quartz and zircon inclusion and reference crystals, collected on two different days with different wavelength lasers, showing typical reproducibilities of $\sim \pm 0.2 \text{ cm}^{-1}$ (2σ) and approximately constant offsets among lasers. Colors of symbols and lines correspond with laser color (excitation wavelength). Circles = inclusion; squares = reference crystal. Solid lines = inclusion means; dashed lines = reference means. Values with errors represent mean peak positions with two sigma standard deviations. A) Quartz 464 cm^{-1} peak. B) Zircon 1008 cm^{-1} peak.

Differences in Peak Positions Using Different Lasers

Using the same data, we compared the difference in peak positions as measured using different laser sources. For quartz, we used the 128 cm^{-1} and the 464 cm^{-1} peaks; for zircon, we used the 975 cm^{-1} and the 1008 cm^{-1} peaks. The measurements were temporally interspersed but are divided in the figures to facilitate comparisons. In principle, if there was no difference in values of the Raman peaks using different lasers, the difference between these peaks would be 0. Peak positions are systematically shifted when comparing green and blue lasers (Figures 13A and 14A), blue and red lasers (Figures 13B and 14B), and green and red lasers (Figures 13C and 14C) for measurements on quartz and zircon reference crystals. For both quartz and zircon, using the red laser source results in the highest peak positions (shifts are positive in plots 13B, 14B and negative in plots 13C, 14C) among the three lasers. Conversely, the green laser source results in the lowest peak positions, with the exception of the 128 cm^{-1} peak differences (Figure 13A). The peak position data show fewer variations for the reference crystals than for the inclusions. The difference in peak position between green and red lasers is more reproducible than the other two laser sources (Figure 13C). Values are more similar for reference crystals when comparing the values of the 128 cm^{-1} peak differences and 464 cm^{-1} peak differences, except for reference crystal measurements of the 128 cm^{-1} peak position for green vs. blue laser (Figure 13A). For zircon, both reference and inclusion crystals show similar variations (Figure 14), but the reference crystal analyses still show less variability than the inclusion analyses.

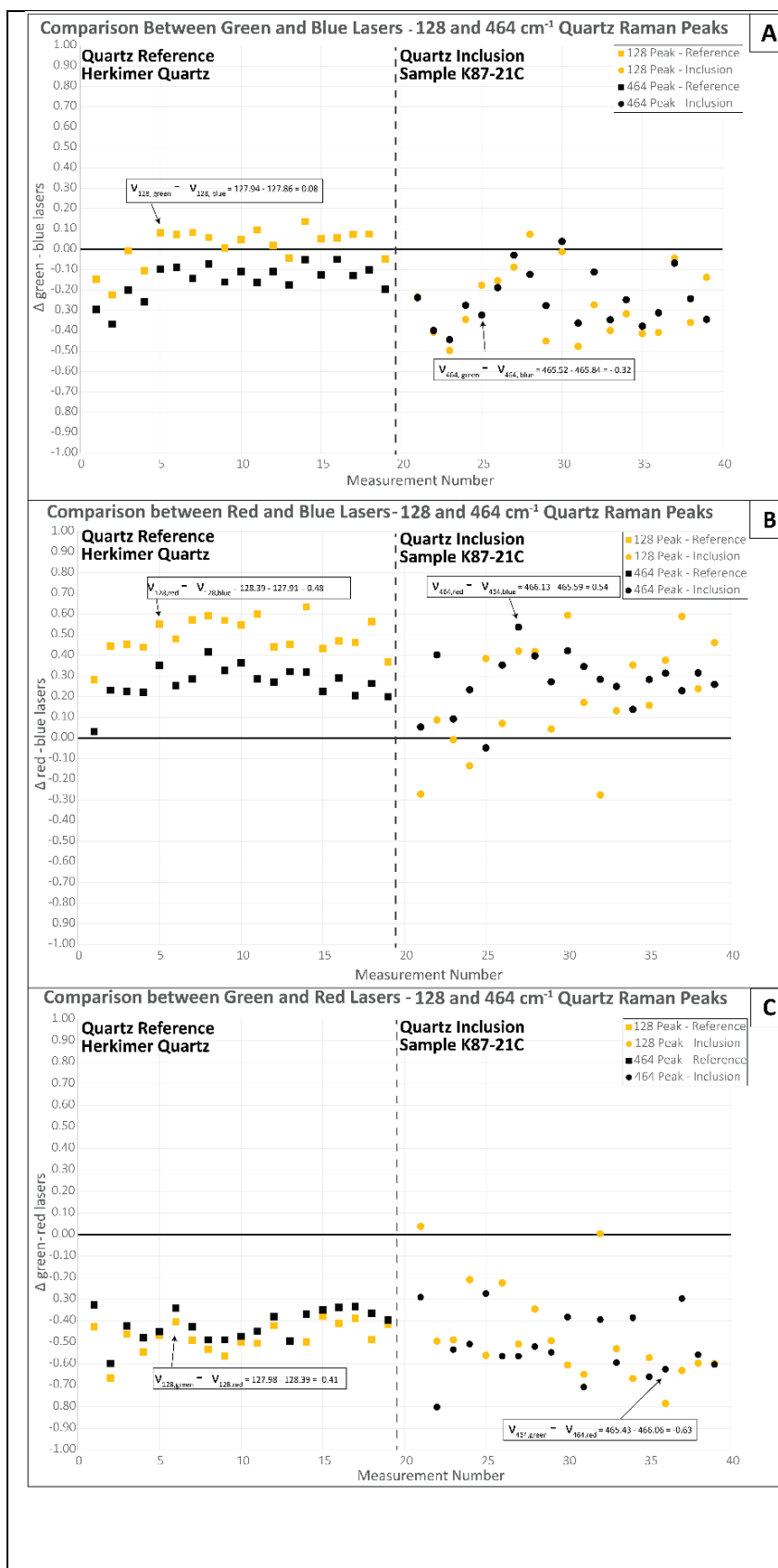


Figure 13. Time-series of the difference in the 128 cm⁻¹ peak positions and the difference in the 464 cm⁻¹ peak positions in quartz as measured using different laser sources (e.g., green vs. blue, blue vs. red, etc.). Example calculation is shown for reference and inclusion in each panel. Measurements of reference and inclusion were interspersed but are separated to facilitate comparisons. The split between reference and inclusion analyses does not represent a shift in instrument behavior. Circles = inclusions; squares = reference crystals. Yellow = 128 cm⁻¹ peaks; black = 464 cm⁻¹ peaks. A) Green vs. blue lasers. B) Blue vs. red lasers. C) Green vs. red lasers. Quartz reference has a better reproducibility than quartz inclusion, and systematic shifts occur to the peak positions for the two lasers.



Figure 14. Time-series of the difference in the 975 cm⁻¹ peak positions and the difference in the 1008 cm⁻¹ peak positions in zircon as measured using different laser sources. Example calculation is shown for reference and inclusion in each panel.

Measurements of reference and inclusion were interspersed but are separated to facilitate comparisons. The split between reference and inclusion analyses does not represent a shift in instrument behavior. Circles = inclusions; squares = reference crystals. Yellow = 975 cm⁻¹ peaks; black = 1008 cm⁻¹ peaks. A) Green vs. blue lasers. B) Blue vs. red lasers. C) Green vs. red lasers. Zircon reference has a better reproducibility than zircon inclusion, and systematic shifts occur to the peak positions for the two lasers.

Quartz Entrapment Pressure Using Different Lasers

P_{trap} values for a single inclusion from sample K87-21C are highest (0.64 to 1.42 GPa, mean = 1.00 GPa) when calculated from measurements collected with the red laser and using 128 cm^{-1} and 464 cm^{-1} peaks (Figure 15; Table 2). Measurements taken with blue and green laser sources show similar P_{trap} values to each other and range between 0.61 and 0.74 GPa. For comparison, Kohn et al. (1992) suggest a garnet nucleation pressure of ca. 0.3 GPa at 450°C, so all calculated P_{trap} values are much higher than inferred from mineral chemistry. Calculations using the red laser data scatter more than for the other two laser sources: ± 0.46 GPa (red) vs. ± 0.03 (green) and ± 0.07 GPa (blue).

Table 2 shows the average $\pm 2\sigma$ values for P_{inc} and P_{trap} as calculated using different combinations of peaks collected with the blue, green, and red lasers. Using the Hg-line as a reference produces nearly the same results as using spectra from a quartz reference crystal. All averages with the blue laser are between 0.63 and 0.69 GPa, regardless of how many peaks were used to calculate P_{inc} , but calculations using the two 128 and 464 cm^{-1} peaks alone have much higher variability than using other combinations of peaks. For the green laser, P_{trap} values range from 0.60 to 0.66 GPa, except when using the two 128 cm^{-1} and 464 cm^{-1} peaks alone. This 128 cm^{-1} and 464 cm^{-1} peak combination for the green laser results in higher P_{trap} values (c. 0.9 GPa), similar to results using the red laser (c. 1.0 GPa), but much higher than nearly all other calculations. Overall, our results show an internal reproducibility of < 0.1 GPa for P_{trap} among the blue and green lasers using a variety of peak combinations, but consistently higher P_{trap} in the core of the garnet compared to the results of Kohn et al. (1992).

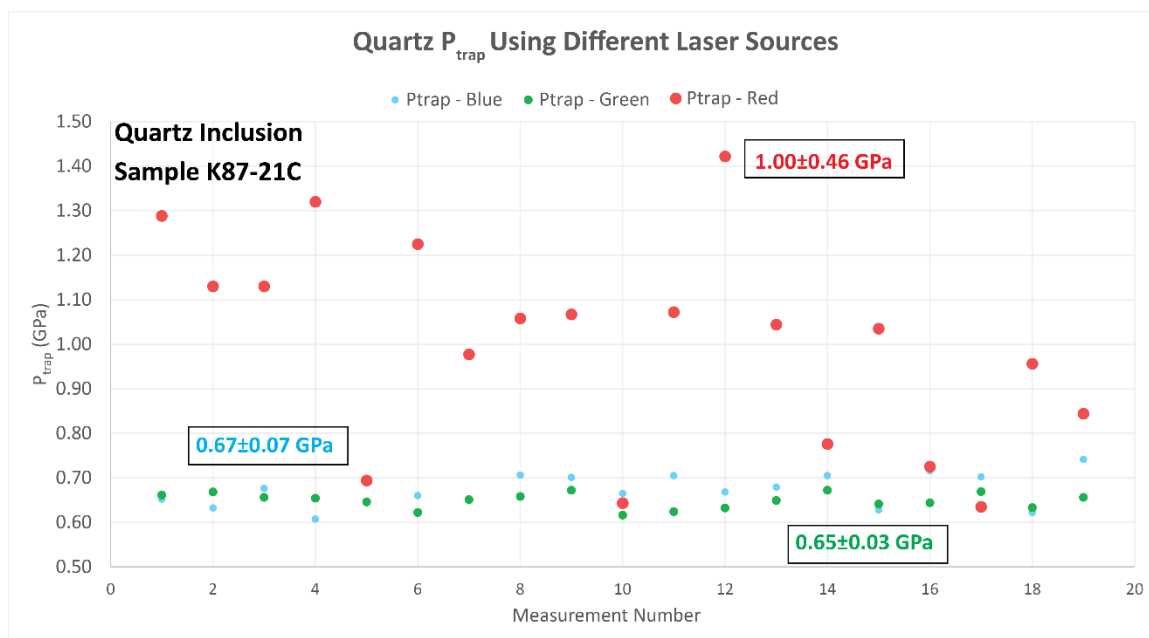


Figure 15. Time-series of quartz entrapment pressures (P_{trap}) using different laser sources. Colors of circles correspond with laser color (excitation wavelength).

P_{trap} calculations using blue and green laser sources show similar values and variabilities (0.67 ± 0.07 GPa for blue, 0.65 ± 0.03 GPa for green). P_{trap} calculations using red laser show much higher overall P_{trap} and variability (1.00 ± 0.46 GPa).

Table 2. Average P_{trap} calculations $\pm 2\sigma$ using a variety of Raman peak combinations with three different laser sources. Raman offsets were obtained using a quartz reference grain (Quartz Ref.) and a Hg-line as reference. Quartz spectra that included the Hg-line were collected on a different day, but values used to calculate Raman offsets can be considered an appropriate representation of using emission lines as an external calibration. P_{inc} calculations using 1 peak used equations from Kohn (2014). All other P_{inc} calculations were made using stRAiMAN (Angel et al., 2019) and an excel spreadsheet provided by M. Alvaro (pers. comm. to MJK, 2018). P_{trap} calculations used EosFit-Pinc (Angel et al., 2017). Low quality spectra for the red laser precluded calculations that used 206 cm^{-1} . Nearly all peak combinations using two distinct calculations for P_{inc} show similar P_{trap} values, except for using two peaks (128 cm^{-1} and 464 cm^{-1}) with the green and red lasers, which resulted in P_{trap} of nearly 1 GPa.

Sample: K87-21 C	Blue Laser	Green Laser	Red Laser
1 peak (128) - Quartz Ref.	0.60±0.05	0.53±0.06	0.53±0.10
1 peak (128) – Hg-line	0.59±0.05	0.52±0.06	0.53±0.08
1 peak (206) - Quartz Ref.	0.63±0.05	0.60±0.02	
1 peak (206) – Hg-line	0.63±0.05	0.60±0.02	
1 peak (464) - Quartz Ref.	0.65±0.03	0.63±0.03	0.65±0.03
1 peak (464) – Hg-line	0.64±0.04	0.62±0.04	0.64±0.03
2 peaks (128-206) – Quartz Ref.	0.67±0.07	0.66±0.03	
2 peaks (128-206) – Hg-line	0.67±0.07	0.66±0.03	
2 peaks (128-464)– Quartz Ref	0.67±0.21	0.87±0.30	1.00±0.46
2 peaks (128-464) – Hg-line	0.69±0.21	0.93±0.16	0.99±0.40
2 peaks (206-464) – Quartz Ref	0.67±0.07	0.64±0.04	
2 peaks (206-464)– Hg-line	0.67±0.07	0.64±0.04	
3 peaks (128-206-464)– Quartz Ref.	0.68±0.07	0.65±0.03	
3 peaks (128-206-464) – Hg-line	0.67±0.07	0.65±0.03	

Summary of Reproducibilities

There are many possible measures of peak position reproducibility, ranging from the precision of numerically fitting a peak position to a measured spectrum, to the variation observed over minutes, hours, or days for a single set of analytical conditions.

Some key measures (all errors at 2σ) include:

1. Numerical accuracy of our peak fitting routines: $\leq \pm 0.02\text{ cm}^{-1}$, as determined through comparison with other software packages.

2. Reproducibility of peak positions over periods of minutes to ~1 hour (short-term stability of instrument): $\sim\pm 0.05 \text{ cm}^{-1}$ as determined from time-series measurements of the same analytical spot during periods of stasis or slow drift (Figure 7).
3. Reproducibility of peak position offsets relative to a fixed reference (484 cm^{-1} Hg line) over periods of minutes to ~1 hour (short-term stability of instrument): $\sim\pm 0.05 \text{ cm}^{-1}$ as determined from time-series measurements of the same analytical spot during periods of stasis or slow drift (Figure 7).
4. Reproducibility of peak positions over periods of tens of minutes (likely analytical conditions): $\leq \sim\pm 0.2 \text{ cm}^{-1}$ as determined from repeated cycling of analyses between reference crystal and inclusion (Figure 12) or from tests of the effects of acquisition time and power density on peak positions (Figure 8). Values vary from day to day.
5. Reproducibility of peak offsets between sample and reference over periods of tens of minutes (likely analytical conditions): $\leq \sim\pm 0.3 \text{ cm}^{-1}$ as determined from the uncertainty in the difference between two measurements, each with uncertainties $\leq \sim\pm 0.2 \text{ cm}^{-1}$.

For use in geobarometry, the reproducibility of calculated P_{trap} is most relevant: ± 0.03 (green laser), ± 0.07 (blue), and ± 0.5 GPa (red), as determined from repeated measurements of reference and sample peak positions (likely analytical conditions; Figure 15).

DISCUSSION

Temporal Drift of Raman Spectra

Understanding the behavior of instruments and laboratory conditions is critical to optimize Raman acquisition measurements and consequently achieve better precision in pressure calculations. Our results show that initial drifting up to 1 cm^{-1} happens for approximately one hour after turning on the lasers (Figure 7). Instrument drifting can happen due to thermal effects on the instrument and changes in the laboratory conditions, such as temperature and electric power (Gaufres et al., 1995; Mestari et al., 1997; Fukura et al., 2006). Furthermore, drifting can also happen due to the repositioning of the monochromator. This drift can significantly change the calculations of P_{trap} of inclusions, depending on calculation methods, which will then alter geological interpretations. Each laser has its own stability period, thus, the time that a laser takes to stabilize will vary depending on the instrument used. For our laboratory settings, the manufacturer recommended waiting times for full laser stability are between 15 and 25 minutes for the 442 nm laser (blue), 1 to 2 minutes for the 532 nm laser (green), and a few minutes for the 633 nm laser (red). Our results indicate that if we follow these guidelines, we will obtain erroneous measurements for initial data collection (Figure 7). We reproduced our measurements with an additional ~ 15 Raman time series experiments, and we observed the same drifting behavior for a minimum of 40 minutes. We did not perform any long-period Raman spectral collection with the red laser, so the long-term stability is unknown. Fukura et al. (2006) found a correlation between peak drift and the

temperature of the CCD detector over a duration of ~1/2 hour after turning on the detector. In our experiments, the CCD detector is continuously thermoelectrically cooled to between -70 and -75 °C, even when the lasers are turned off, suggesting that stabilization of the laser, not CCD, must be responsible for initial drift. We recommend either waiting for approximately one hour after turning on lasers to start Raman spectral collection, regardless of laser wavelength, or simply leaving the laser power supply turned on.

Well-controlled environmental conditions of the laboratory are essential for precise Raman spectral measurements. In addition to CCD stability, oscillations in room temperature have been reported to correlate with oscillations in peak positions (Fukura et al., 2006). We also observe correlations between room temperature and peak position, both during abrupt changes (Figure 16) and small oscillations (Figure 17). Abrupt changes in temperature reflect the HVAC system in the building, especially near 10 PM, when the building changes to “night mode” (allowing a temperature increase up to ~1 °C), and 5-6 AM when it changes back to “day mode” (Figure 18). For laboratories that do not have 24-hour temperature regulation ≤ 0.1 °C, we recommend collecting Raman spectra during normal operation hours, when temperature is most stable. For measurements over longer periods (e.g., 24 hours), monitoring temperature may help identify the largest abrupt shifts and provide approximate corrections.

Atomic emission line spectra (e.g., Hg, Neon) can be used as an independent calibration to check instrument and spectral stability throughout the day (Mestari et al., 1997; Hutsebaut et al., 2005; Odake et al., 2008, Jakubek et al., 2020). Because the drifts of the Hg-line, quartz, and zircon peaks correlate closely (Figure 19), light leakage into

the microscope (e.g., using a smaller magnification or long working-distance objective) could help monitor and correct for abrupt shifts in Raman peak positions. However, temporal shifts to the Hg, quartz, and zircon lines do not correspond precisely, so their offsets are not identical for reference crystal analyses (e.g., Figure 7A, 4:30 to 5:40 AM; Figure 7C, 4:30 to 5:00 AM). Although the changes to the Hg-quartz and Hg-zircon peak offsets are much smaller than individual peak shifts, they would still contribute error on the order of several tenths of a cm^{-1} (Figure 20). We note that use of a larger magnification objective increases the analytical spot size (which may be undesirable), but also increases count rate and P/B. We recommend using emission line spectra to monitor machine stability and as an additional source of reference (e.g., in addition to a crystal), but to check reference crystals periodically, especially after any large shifts to absolute positions of emission line spectra.

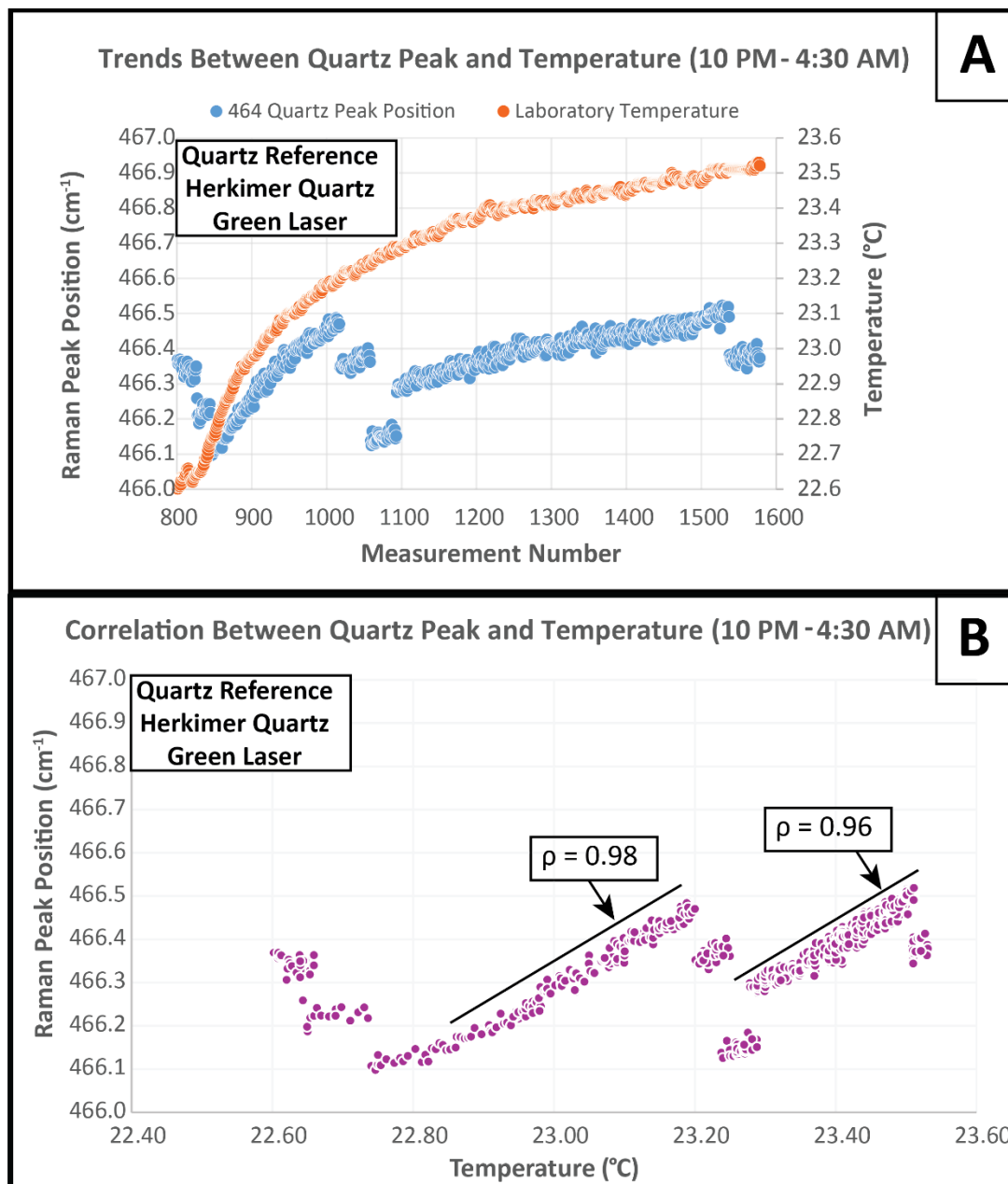


Figure 16. (A) Trends and (B) correlation between quartz 464 cm^{-1} peak and temperature at the Raman laboratory during an abrupt change in temperature at night. Blue dots = quartz peak (cm^{-1}); orange dots = temperature ($^{\circ}\text{C}$). ρ = correlation coefficient. Raman peak positions correlate with temperature over some intervals, but also shift abruptly.

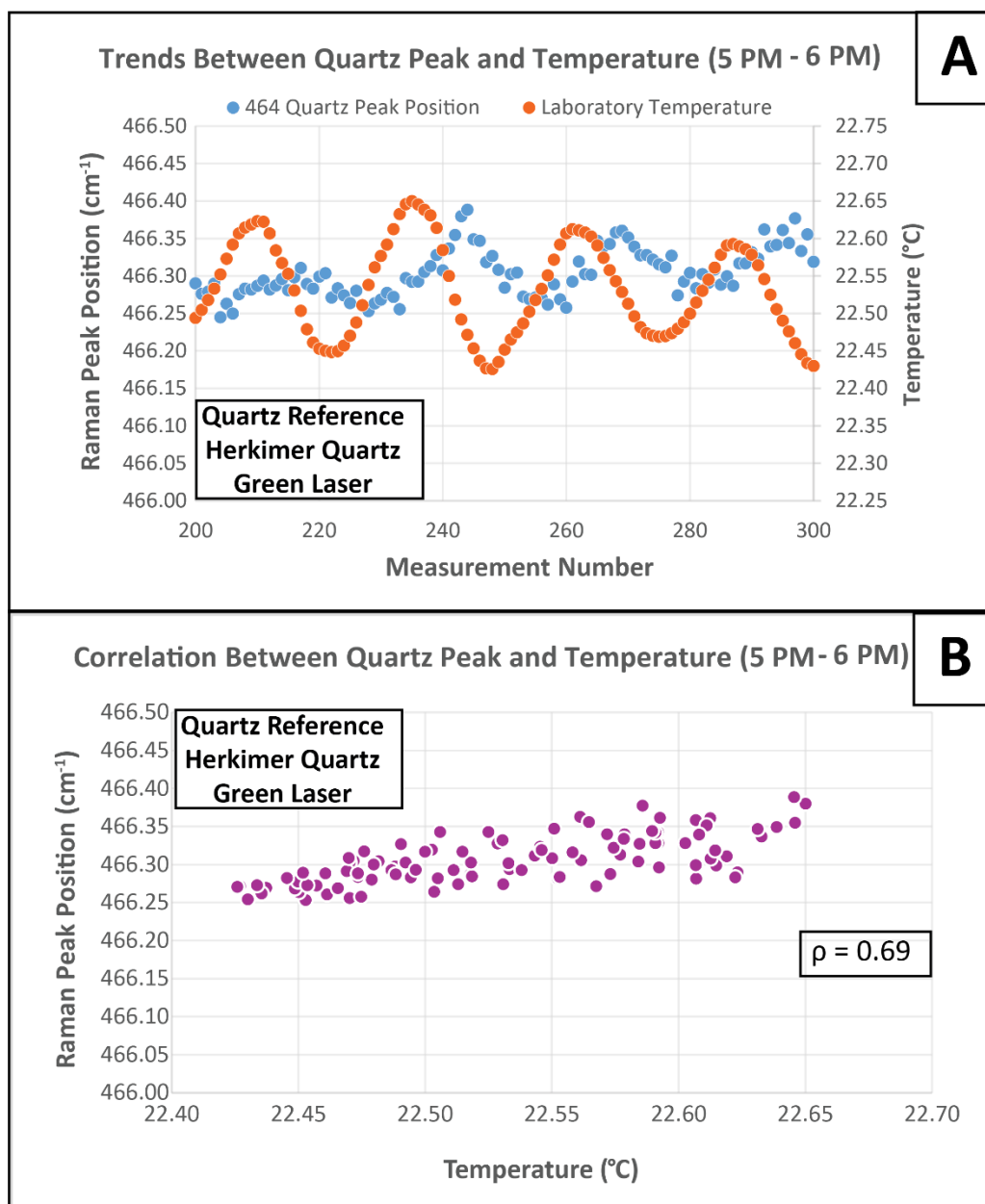


Figure 17. (A) Oscillation in quartz 464 cm^{-1} peak position mimics oscillation in temperature with a time lag of ~ 4.5 minutes. (B) Correlation between quartz 464 cm^{-1} peak and laboratory temperature during a relatively stable period. Correlation was calculated after optimizing time offset between peak and temperature. Blue dots = quartz peak (cm^{-1}); orange dots = temperature ($^{\circ}\text{C}$); ρ = correlation coefficient.

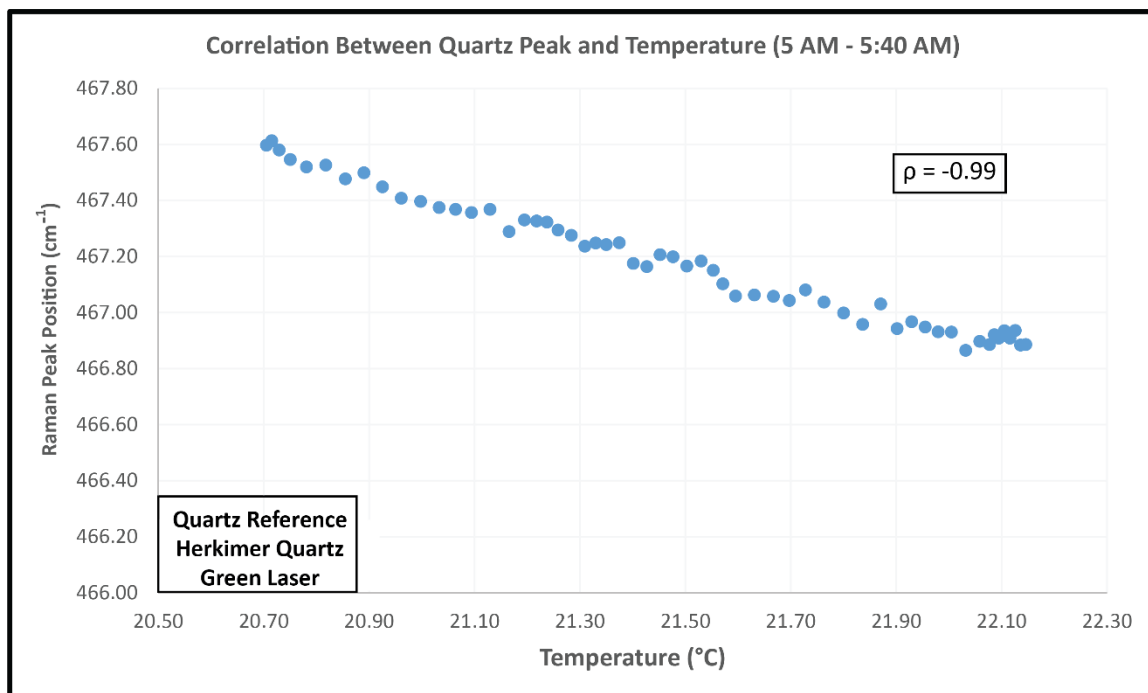


Figure 18. Negative correlation between quartz 464 cm^{-1} peak and laboratory temperature during a rapid change in temperature in the morning. ρ = correlation coefficient.

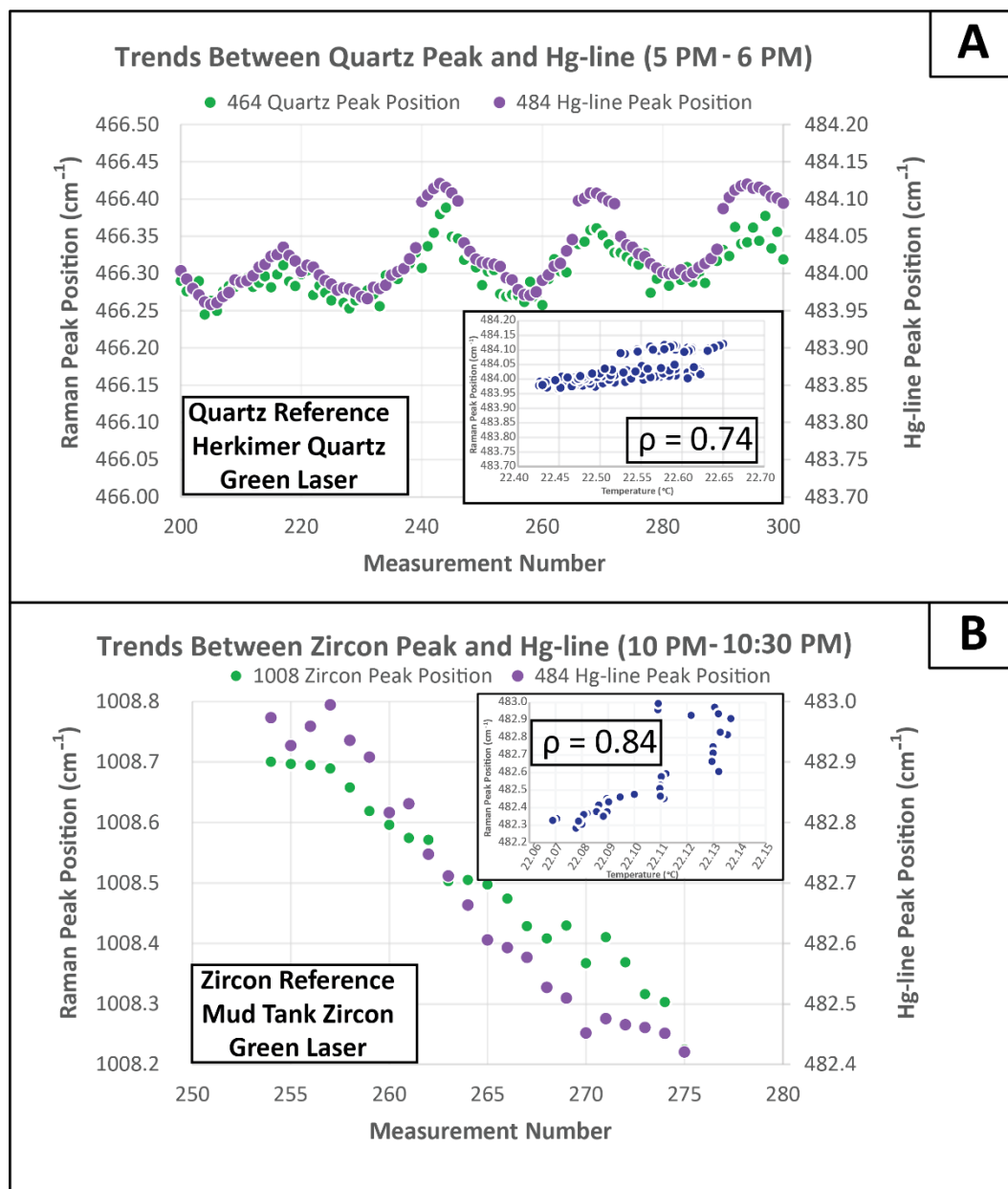


Figure 19. Time-series of Hg-line (purple dots) and quartz or zircon peaks (green dots) and correlations of Hg-line with temperature (inset maps); ρ = correlation coefficient. (A) Quartz. (B) Zircon. We do not know why there are abrupt $\sim 0.05 \text{ cm}^{-1}$ shifts in the Hg-line between measurements 240 and 300 for quartz.

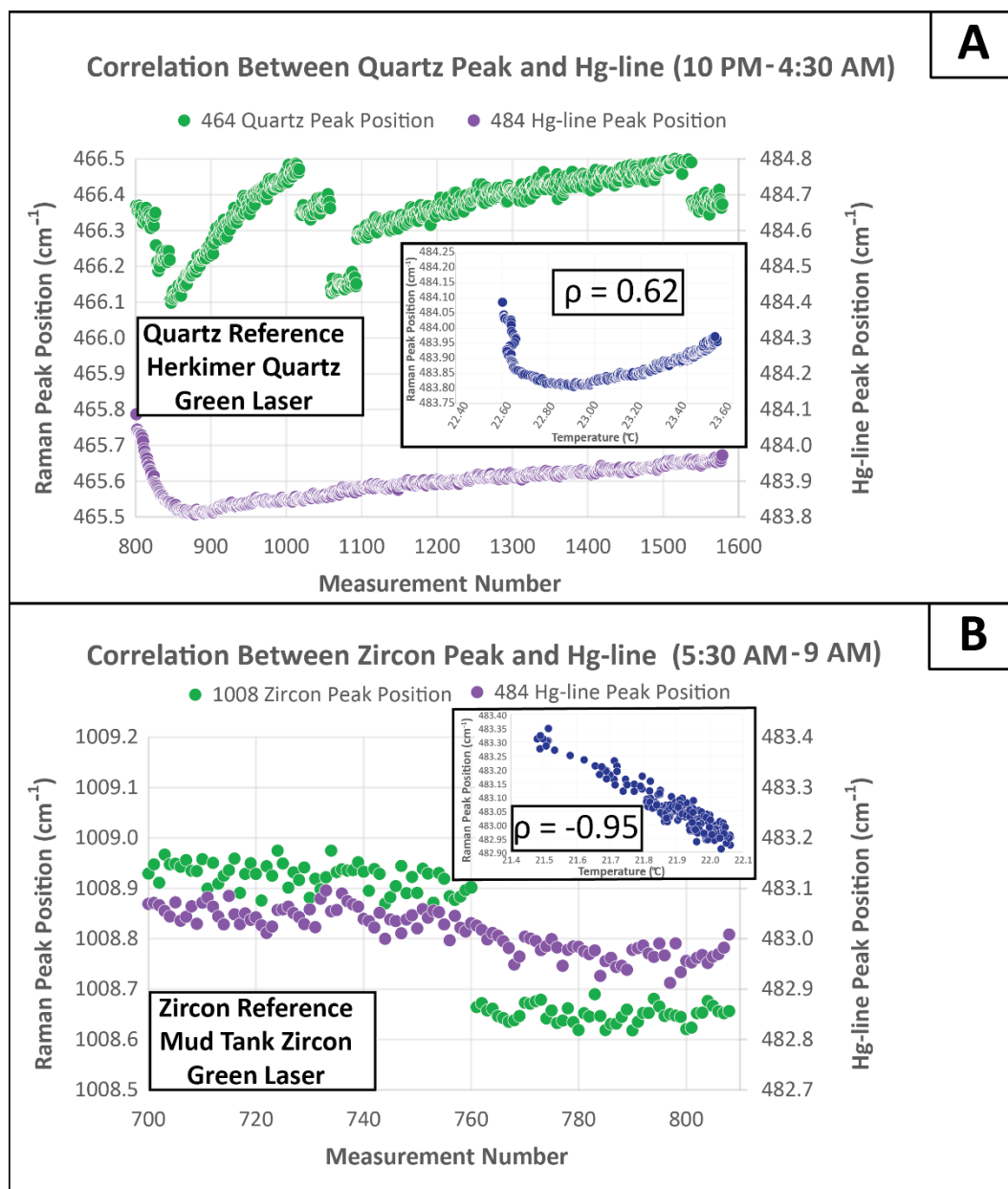


Figure 20. Time-series of Hg-line (purple dots) and quartz or zircon peaks (green dots) and correlations of Hg-line with temperature (inset maps); ρ = correlation coefficient. (A) Quartz. (B) Zircon. Quartz and zircon peaks drift slowly in parallel with the Hg line, but also exhibit 0.1 to 0.4 cm^{-1} jumps independent of the Hg line.

Effects of Power Density and Acquisition Time on Quartz and Zircon

Changes in temperature can alter the position and width of Raman peaks. Also, zircon is highly sensitive to absorbing light of specific frequencies, even at low power densities (5 to 10 $\text{mW}/\mu\text{m}^2$) (Nasdala et al., 1998). Absorption can increase the

temperature in a sample during analysis and temporarily alter band frequencies and widths (Nasdala et al., 1998). Constant peak positions (Figure 8) and FWHM (Figure 10) indicate that quartz inclusions are not susceptible to heating over wide ranging power densities (0.5 to 50 mW) and acquisition times (3-270 sec) for any laser. Similarly, we see no evidence for peak shifts in zircon using a green or red laser (Figures 8, 9). Some of our results for zircon contrast with Zhong et al. (2019), who used the same green laser source (frequency doubled Nd: YAG, 532 nm), but saw peak shifts up to 2 cm^{-1} at power densities $>\sim 10\text{ mW}$. The direction of shift is consistent with an increase in temperature during analysis. With the blue laser, discoloration and damage of zircon inclusions at high power densities (Figure 11) indicates strong coupling between laser and zircon. If a blue laser is used, we recommend using very low power densities ($<\sim 12\text{ mW}$).

The difference in results for our study vs. Zhong et al. (2019) might reflect differences in prior radiation damage. Previous studies have shown that zircons with higher levels of metamictization have different bonding structures that shift and broaden Raman peaks and make them more susceptible to light absorption and heating (e.g., Nasdala et al., 1995 and 1998; Hoskin and Rodgers, 1996; Zhang et al., 2000; Campomenosi et al., 2020). Zircons begin to accumulate α -radiation damage at temperatures below $\sim 230\text{ }^{\circ}\text{C}$ (Pidgeon, 2014) similar to the closure temperature of zircon fission tracks ($\sim 240\text{ }^{\circ}\text{C}$; see Bernet and Garver, 2005). Our sample was metamorphosed at $\sim 40\text{ Ma}$ and cooled through $\sim 240\text{ }^{\circ}\text{C}$ by $\sim 33\text{ Ma}$ (Amato et al., 1999). Consequently, radiation damage could have accumulated for no more than 33 Myr. In contrast, the rocks that Zhong et al. (2019) analyzed, from the Bergen Arcs, Norway, were metamorphosed at 425-430 Ma and cooled below $250\text{ }^{\circ}\text{C}$ probably by 300 Ma, and certainly by 250 Ma

(Dunlap and Fossen, 1998). While we do not know the U and Th concentration in each zircon inclusion, the magnitude of metamictization of the zircons analyzed by Zhong et al. (2019) was likely many times larger than in our rocks, possibly making the Bergen Arcs zircons more susceptible to laser heating. If so, analysis of young zircons with low degrees of radiation damage, such as in our samples, may permit use of higher laser power and longer acquisition times. Trace elements show a wide range of light absorption characteristics, so differences in trace element contents (e.g., HREE) might also cause differences in laser absorption and heating. Because U and HREE contents vary considerably among zircon crystals, susceptibility to heating must be highly specific to each zircon crystal.

Zircon Damage Using Blue Laser Source

One peculiarity in our study was the ability to damage four zircon inclusions using the blue laser source (442 nm), even with low ND filters (e.g., 1%). The sensitivity of the Raman signal to the blue laser allowed us to collect high-quality spectra of zircon inclusions using a 1% ND filter and 3 seconds of acquisition. Unlike the green and red lasers, which show no dependence of spectra or physical appearance of crystals with variations in laser intensity, increasing laser power caused zircon inclusions to become discolored (Figure 11). Most likely, these zircons absorbed more radiation at 442 nm and consequently heated, even though at low intensities there was no obvious change to peak positions. Evidently, the red and green laser sources did not heat the zircons appreciably, unlike in the study of Zhong et al. (2019).

Repeat experiments using the blue laser to analyze zircon did not reproduce our original results – no zircon was damaged. Rather, we observed lower Raman scattering

intensities, and no discoloration. The failure of our repeat experiments may be related to changes in the laser alignment. Each laser possesses its own coupling mirrors that conduct the light into the Raman system. Misalignment in the mirrors will reduce the laser flux to the sample, resulting in less heating (if heating is occurring) and a reduced Raman signal. Alternatively, the output power of the He: Cd used on the blue laser could decrease with time. A much lower signal intensity during the repeat experiments is consistent with either of these explanations.

Overall, using shorter excitation wavelengths, such as the 442 nm laser, yields higher Raman scattering intensity and lower acquisition times, as expected as Raman scattering intensity should scale inversely to the fourth power of the excitation wavelength (McCreery, 2000). Using the blue laser source results in faster spectral collection because it 1) covers a wider spectral range, 2) produces higher quality spectra, and 3) has a higher peak-to-background ratio. However, the laser must be checked *a priori* to establish which power setting will not irreversibly alter zircon inclusions.

Effect of Laser Frequency on Raman Spectrum Quality

The similar reproducibilities of peak positions using different lasers (Figure 15) might at first suggest that use of different lasers would not change geologic interpretations significantly. However, reproducibility does not equate to accuracy, and systematic offsets between Raman spectra collected with different lasers could occur. Although others have tested how different excitation wavelengths in biological samples affect the quality of Raman spectra (Sato et al., 2001; Kerr et al., 2015), we know of no comparable studies for geologic samples. In theory, the inverse relationship between wavelength and spectral resolution implies that use of longer wavelength lasers (633 in

this study) should produce more highly resolved spectra than shorter wavelength lasers (442 in this study). However, the blue laser source yields higher Raman scattering intensities and higher peak-to-background ratios than the red laser, offsetting theoretical disadvantages.

Longer excitation wavelengths generally cause lower fluorescence although the Raman intensity is weaker (McCreery, 2000). For zircon, use of the longest wavelength laser source (red, 633 nm) produced high-quality spectra, although with lower Raman intensities compared to the other lasers (Figure 21). An advantage of using the red laser is that the garnet peaks at ca. 350 and 900 cm^{-1} are smaller in comparison to spectra collected using the blue and green laser sources. Consequently, any spectral corrections for overlapping garnet peaks would be smaller.

In principle, the Raman shifts observed in a sample should be independent of the laser used to collect the spectrum, but we obtain different Raman peak positions when using different laser sources. We cannot offer any definitive explanation, but note that large shifts to the monochromator to accommodate the different excitation wavelengths might introduce systematic shifts on the order of cm^{-1} 's. We do not ascribe any special significance to these differences. Note that the large shifts that we observed in our time series data do not result from repositioning the monochromator.

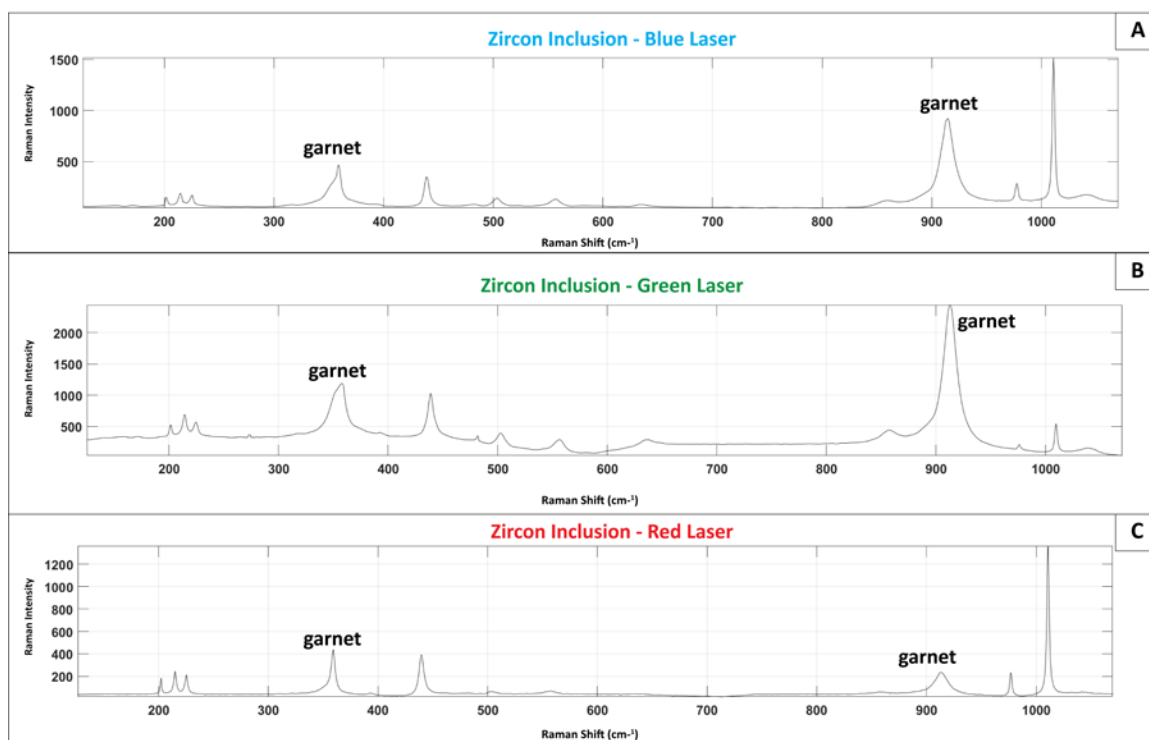


Figure 21. Raman spectra of a single zircon inclusion using different lasers. (A) blue. (B) green. (C) red. The spectra were collected sequentially with the same parameters. All three lasers show well-resolved peaks, but the red laser shows the smallest garnet intensities and highest zircon P/B, while the green laser shows the largest garnet and lowest zircon intensities. All unlabeled peaks are characteristic of zircon.

Effect of Different Lasers on Calculated P_{trap} in Quartz

Many barometric studies use a green laser source (~532 nm e.g., Enami et al., 2007; Kouketsu et al., 2014; Ashley et al., 2014, 2015, 2017; Thomas and Spear, 2018; Gonzalez et al., 2019; Zhong et al., 2019) because it is readily available, relatively inexpensive, and produces good spectral resolution for geologic samples. For inclusion elastic barometry, calculated P_{trap} can be sensitive to small shifts in Raman peak positions depending on the method used. Consequently, the large abrupt shifts in peaks that we observe due to machine instability could be misconstrued to represent large differences in P_{trap} . For example, if an offset of 1.5 cm^{-1} of the 464 cm^{-1} peak is used to calculate P_{inc} , using the garnet-quartz equation from Kohn (2014) at $450 \text{ }^{\circ}\text{C}$, we obtain a P_{inc} of 0.17

GPa and P_{trap} of ~ 0.71 GPa. If we add 1 cm^{-1} to this offset (e.g., an abrupt peak shift), the new calculated P_{inc} is 0.28 and P_{trap} is ~ 0.89 GPa. Thus, systematic errors in P_{trap} up to 0.1 to 0.2 GPa could result from changes in peak positions caused by machine instability.

Calculated P_{trap} can vary depending on which laser source and Raman peaks are used. For instance, red and green laser sources yield a significantly higher calculated P_{trap} compared to the blue laser in Table 2, but only when using a two-peak combination of the 128 cm^{-1} and 464 cm^{-1} peaks. Apparently, P_{trap} can be sensitive to omission of the 206 cm^{-1} mode. The good consistency and small variability in calculated P_{trap} using the blue and green lasers generally reflects well resolved Raman peaks and high P/B ratio. While either laser could be used for QuiG barometry, other minerals could experience heating (e.g., metamict zircon) or fluorescence (kyanite; M Kohn, unpublished data). Thus, it is important to test different laser sources on each specific mineral to determine which laser will optimize Raman scattering intensities and P/B ratios without encountering fluorescence. We recommend using the blue laser for QuiG barometry because it is the most consistent of the three lasers presented in this study.

CONCLUSIONS

Understanding what influences the reproducibility of Raman spectra of mineral inclusions is essential to achieve optimal P-T calculations in elastic geothermobarometry. In this work, we demonstrated the main factors that will induce major changes in Raman peak positions in quartz and zircon inclusion and reference crystals. Machine instability as well as external factors, such as temperature variations greater than 0.1 °C, can cause significant shifts in Raman peak positions that will compromise accurate P_{trap} values. To mitigate these effects, we recommend:

- 1- waiting for approximately one hour after turning on lasers to collect Raman spectra or keeping the lasers on at all times;
- 2- collecting Raman spectra during normal operation hours, where temperature variation is minimal, or monitoring temperature in the laboratory room to identify significant shifts;
- 3- using emission line spectra (e.g., Hg-line) in addition to a reference crystal to check machine stability and make drift corrections.

Overall, varying power density or acquisition time does not induce significant peak shifts for quartz and zircon using either green or blue lasers. In addition, the blue laser provides the best spectral resolution and peak-to-background ratio, but such small wavelengths can damage zircon, probably because of overheating. Trace element contents, as well as the amount of radiation damage, might cause differential laser absorption and heating among zircon grains, so we recommend using very low power

densities ($< \sim 12$ mW) with the blue lasers. Further studies could focus on what causes damage to zircons using a blue laser source.

The blue laser source gives the most reproducible results for all methods of estimating P_{trap} , and we recommend using this laser, if available, for analysis of quartz and zircon. Use of the red and green laser is acceptable, but only for specific methods of calculating P_{trap} .

Lastly, establishing community norms for data collection are essential to improve Raman measurements and reduce uncertainties in P-T estimates. In addition to parameters that are commonly reported (e.g., microscope model, objective, grating, focal length, laser type, power, and wavelength, confocal aperture diameter, slit size, spectral range and resolution, spot size, acquisition time), reports should include:

- 1- Number of inclusions being analyzed
- 2- Frequency of machine calibration
- 3- Variation in room temperature
- 4- Frequency of reference crystal spectral collection. If an external reference is not collected with every spectrum (e.g., Hg-line), we recommend measuring a reference spectrum within 10 minutes of measuring unknowns to correct for peak drift
- 5- Peak position reproducibility for all relevant peaks
- 6- Propagated reproducibility in P_{inc}
- 7- Propagated reproducibility in P_{trap}

These recommendations will improve data collection reporting and will contribute to more detailed reports on uncertainties in P-T estimates using Raman microspectroscopy.

REFERENCES

- Adams, H.G., Cohen, L.H., and Rosenfeld, J.L., 1975, Solid inclusion piezothermometry I: Comparison dilatometry: *American Mineralogist*, v. 60, p. 574–583
- Amato, J.M., Johnson, C.M., Baumgartner, L.P., and Beard, B.L., 1999, Rapid exhumation of the Zermatt-Saas ophiolite deduced from high-precision SmNd and RbSr geochronology: *Earth and Planetary Science Letters*, v. 171, p. 425–438, doi:10.1016/s0012-821x(99)00161-2.
- Angel, R.J., Mazzucchelli, M.L., Alvaro, M., and Nestola, F., 2017, EosFit-Pinc: A simple GUI for host-inclusion elastic thermobarometry: *American Mineralogist*, v. 102, p. 1957–1960, doi:10.2138/am-2017-6190.
- Angel, R.J., Mazzucchelli, M.L., Alvaro, M., Nimis, P., and Nestola, F., 2014, Letter. Geobarometry from host-inclusion systems: The role of elastic relaxation: *American Mineralogist*, v. 99, p. 2146–2149, doi:10.2138/am-2014-5047.
- Angel, R.J., Murri, M., Mihailova, B., and Alvaro, M., 2019, Stress, strain and Raman shifts: *Zeitschrift für Kristallographie - Crystalline Materials*, v. 234, p. 129–140, doi:10.1515/zkri-2018-2112.
- Ashley, K.T., Barkoff, D.W., and Steele-MacInnis, M., 2017, Barometric constraints based on apatite inclusions in garnet: *American Mineralogist*, v. 102, p. 743–749, doi:10.2138/am-2017-5898.
- Ashley, K.T., Caddick, M.J., Steele-MacInnis, M.J., Bodnar, R.J., and Dragovic, B., 2014, Geothermobarometric history of subduction recorded by quartz inclusions in garnet: *Geochemistry, Geophysics, Geosystems*, v. 15, p. 350–360, doi:10.1002/2013gc005106.

- Ashley, K.T., Darling, R.S., Bodnar, R.J., and Law, R.D., 2015, Significance of “stretched” mineral inclusions for reconstructing P–T exhumation history: *Contributions to Mineralogy and Petrology*, v. 169, p. 55, doi:10.1007/s00410-015-1149-0.
- Al-Rumaithi, A., 2020. Raman Spectrum Baseline Removal (<https://www.mathworks.com/matlabcentral/fileexchange/69649-raman-spectrum-baseline-removal>), MATLAB Central File Exchange. Retrieved September 8, 2020.
- Bernet, M., and Garver, J.I., 2005, Fission-track Analysis of Detrital Zircon: Reviews in *Mineralogy and Geochemistry*, v. 58, p. 205–237, doi:10.2138/rmg.2005.58.8.
- Beyssac, O., Rouzaud, J.-N., Goffé, B., Brunet, F., and Chopin, C., 2002, Graphitization in a high-pressure, low-temperature metamorphic gradient: a Raman microspectroscopy and HRTEM study: *Contributions to Mineralogy and Petrology*, v. 143, p. 19–31, doi:10.1007/s00410-001-0324-7.
- Campomenosi, N., Rubatto, D., Hermann, J., Mihailova, B., Scambelluri, M., and Alvaro, M., 2020, Establishing a protocol for the selection of zircon inclusions in garnet for Raman thermobarometry: *American Mineralogist*, v. 105, p. 992–1001, doi:10.2138/am-2020-7246.
- Castro, A.E., and Spear, F.S., 2016, Reaction overstepping and re-evaluation of peak P–T conditions of the blueschist unit Sifnos, Greece: implications for the Cyclades subduction zone: *International Geology Review*, v. 59, p. 1–15, doi:10.1080/00206814.2016.1200499.
- Dunlap, W.J., and Fossen, H., 1998, Early Paleozoic orogenic collapse, tectonic stability, and late Paleozoic continental rifting revealed through thermochronology of K-feldspars, southern Norway: *Tectonics*, v. 17, p. 604–620, doi:10.1029/98tc01603.
- Enami, M., Nishiyama, T., and Mouri, T., 2007, Laser Raman microspectrometry of metamorphic quartz: A simple method for comparison of metamorphic pressures: *American Mineralogist*, v. 92, p. 1303–1315, doi:10.2138/am.2007.2438.

- Fukura, S., Mizukami, T., Odake, S., and Kagi, H., 2006, Factors Determining the Stability, Resolution, and Precision of a Conventional Raman Spectrometer: *Applied Spectroscopy*, v. 60, p. 946–950, doi:10.1366/000370206778062165.
- Gaufrès, R., Huguet, P., and Arab, Y., 1995, Method for the determination of spectral shifts in Raman spectroscopy: *Journal of Raman Spectroscopy*, v. 26, p. 243–253, doi:10.1002/jrs.1250260307.
- Gonzalez, J.P., Thomas, J.B., Baldwin, S.L., and Alvaro, M., 2019, Quartz-in-garnet and Ti-in-quartz thermobarometry: Methodology and first application to a quartzofeldspathic gneiss from eastern Papua New Guinea: *Journal of Metamorphic Geology*, v. 37, p. 1193–1208, doi:10.1111/jmg.12508.
- Hoskin, P. and K. Rodgers. “Raman spectral shift in the isomorphous series (Zr_{1-x}Hf_x) SiO₄.” (1996).
- Hutsebaut, D., Vandenabeele, P., and Moens, L., 2005, Evaluation of an accurate calibration and spectral standardization procedure for Raman spectroscopy: *Analyst*, v. 130, p. 1204–1214, doi:10.1039/b503624k.
- Jakubek, R.S., and Fries, M.D., 2020, Calibration of Raman wavenumber in large Raman images using a mercury-argon lamp: *Journal of Raman Spectroscopy*, v. 51, p. 1172–1185, doi:10.1002/jrs.5887.
- Kerr, L.T., Byrne, H.J., and Hennelly, B.M., 2015, Optimal choice of sample substrate and laser wavelength for Raman spectroscopic analysis of biological specimen: *Analytical Methods*, v. 7, p. 5041–5052, doi:10.1039/c5ay00327j.
- Kohn, M.J., 2014, “Thermoba-Raman-try”: Calibration of spectroscopic barometers and thermometers for mineral inclusions: *Earth and Planetary Science Letters*, v. 388, p. 187–196, doi:10.1016/j.epsl.2013.11.054.
- Kohn, M.J., Orange, D.L., Spear, F.S., Rumble, D., and Harrison, T.M., 1992, Pressure, Temperature, and Structural Evolution of West-Central New Hampshire: Hot Thrusts over Cold Basement: *Journal of Petrology*, v. 33, p. 521–556, doi:10.1093/petrology/33.3.521.

- Korsakov, A.V., Perraki, M., Zhukov, V.P., Gussem, K.D., Vandenabeele, P., and Tomilenko, A.A., 2009, Is quartz a potential indicator of ultrahigh-pressure metamorphism? Laser Raman spectroscopy of quartz inclusions in ultrahigh-pressure garnets: *European Journal of Mineralogy*, v. 21, p. 1313–1323, doi:10.1127/0935-1221/2009/0021-2006.
- Kouketsu, Y., Nishiyama, T., Ikeda, T., and Enami, M., 2014, Evaluation of residual pressure in an inclusion–host system using negative frequency shift of quartz Raman spectra: *American Mineralogist*, v. 99, p. 433–442, doi:10.2138/am.2014.4427.
- Mccreery, Richard. (2000). Raman Spectroscopy for Chemical Analysis. 10.1088/0957-0233/12/5/704.
- Mernagh, T.P., and Wilde, A.R., 1989, The use of the laser Raman microprobe for the determination of salinity in fluid inclusions: *Geochimica et Cosmochimica Acta*, v. 53, p. 765–771, doi:10.1016/0016-7037(89)90022-7.
- Mestari, A., Gauffrès, R., and Huguet, P., 1997, Behaviour of the calibration of a Raman spectrometer with temperature changes: *Journal of Raman Spectroscopy*, v. 28, p. 785–789, doi:10.1002/(sici)1097-4555(199710)28:10<785::aid-jrs148>3.0.co;2-d.
- Nasdala, L., Irmer, G., and Wolf, D., 1995, The degree of metamictization in zircon: a Raman spectroscopic study: *European Journal of Mineralogy*, v. 7, p. 471–478, doi:10.1127/ejm/7/3/0471.
- Nasdala, L., Pidgeon, R.T., Wolf, D., and Irmer, G., 1998, Metamictization and U-PB isotopic discordance in single zircons: a combined Raman microprobe and SHRIMP ion probe study: *Mineralogy and Petrology*, v. 62, p. 1–27, doi:10.1007/bf01173760.
- Odake, S., Fukura, S., and Kagi, H., 2008, High Precision in Raman Frequency Achieved Using Real-Time Calibration with a Neon Emission Line: Application to Three-Dimensional Stress Mapping Observations: *Applied Spectroscopy*, v. 62, p. 1084–1087, doi:10.1366/000370208786049169.

- Pidgeon, R.T., 2014, Zircon radiation damage ages: *Chemical Geology*, v. 367, p. 13–22, doi:10.1016/j.chemgeo.2013.12.010.
- Rosasco, G.J., Roedder, E., and Simmons, J.H., 1975, Laser-Excited Raman Spectroscopy for Nondestructive Partial Analysis of Individual Phases in Fluid Inclusions in Minerals: *Science*, v. 190, p. 557–560, doi:10.1126/science.190.4214.557.
- Rosenfeld, J.L., and Chase, A.B., 1961, Pressure and temperature of crystallization from elastic effects around solid inclusions in minerals? *American Journal of Science*, v. 259, p. 519–541, doi:10.2475/ajs.259.7.519.
- Sato, H., Chiba, H., Tashiro, H., and Ozaki, Y., 2001, Excitation wavelength-dependent changes in Raman spectra of whole blood and hemoglobin: comparison of the spectra with 514.5-, 720-, and 1064-nm excitation: *Journal of Biomedical Optics*, v. 6, p. 366–370, doi:10.1117/1.1380668.
- Schmidt, C., and Ziemann, M.A., 2000, In-situ Raman spectroscopy of quartz: A pressure sensor for hydrothermal diamond-anvil cell experiments at elevated temperatures: *American Mineralogist*, v. 85, p. 1725–1734, doi:10.2138/am-2000-11-1216.
- Sobolev, N.V., and Shatsky, V.S., 1990, Diamond inclusions in garnets from metamorphic rocks: a new environment for diamond formation: *Nature*, v. 343, p. 742–746, doi:10.1038/343742a0.
- Spear, F.S., Thomas, J.B., and Hallett, B.W., 2014, Overstepping the garnet isograd: a comparison of QuiG barometry and thermodynamic modeling: *Contributions to Mineralogy and Petrology*, v. 168, p. 1059, doi:10.1007/s00410-014-1059-6.
- Thomas, J.B., and Spear, F.S., 2018, Experimental study of quartz inclusions in garnet at pressures up to 3.0 GPa: evaluating validity of the quartz-in-garnet inclusion elastic thermobarometer: *Contributions to Mineralogy and Petrology*, v. 173, p. 42, doi:10.1007/s00410-018-1469-y.

- Wahadoszamen, Md., Rahaman, A., Hoque, N.Md.R., Talukder, A.I., Abedin, K.M., and Haider, A.F.M.Y., 2015, Laser Raman Spectroscopy with Different Excitation Sources and Extension to Surface Enhanced Raman Spectroscopy: *Journal of Spectroscopy*, v. 2015, p. 1–8, doi:10.1155/2015/895317.
- Zhang, M., Salje, E.K.H., Farnan, I., Graeme-Barber, A., Daniel, P., Ewing, R.C., Clark, A.M., and Leroux, H., 2000, Metamictization of zircon: Raman spectroscopic study: *Journal of Physics: Condensed Matter*, v. 12, p. 1915, doi:10.1088/0953-8984/12/8/333.
- Zhong, X., Andersen, N.H., Dabrowski, M., and Jamtveit, B., 2019, Zircon and quartz inclusions in garnet used for complementary Raman thermobarometry: application to the Holsnøy eclogite, Bergen Arcs, Western Norway: *Contributions to Mineralogy and Petrology*, v. 174, p. 50, doi:10.1007/s00410-019-1584-4.